Utrecht University

Institute for Marine and Atmospheric Research Utrecht (IMAU)

Royal Netherlands Meteorological Institute (KNMI)

# Detecting and forecasting large hail in the Netherlands

*Author:*
Casper Kalkhoven

*Supervisors:*
Dr. Aarnout van Delden
Dr. Sander Tijm

August 7, 2017

**Utrecht University**

Royal Netherlands
Meteorological Institute
*Ministry of Infrastructure and the Environment*

# Abstract

In this thesis, the Hail Detection Algorithm (HDA) developed by Witt et al. [1998] is used to detect large hail. This algorithm is based on single-polarization radar and NWP model data and gives an estimate of the Maximum Expected Hail Size (MEHS). Some difficulties like the occurrence of ground clutter and storm tilt were encountered while applying the HDA, but eventually methods have been developed to overcome these problems. Using the outcomes of the algorithm, a climatology has been made for the Netherlands for the time that the volume data of the two KNMI radars (De Bilt and Den Helder) has been archived (2008-2016). Also, the HDA is used in a case study of 23rd of June 2016, where a single hail storm caused over 500 million euros of damage to houses, cars and agricultural properties. To prevent severe damage in the future, it is of great importance that one can indicate whether or not hail will occur in a certain situation. Moreover, one ideally wants information about the hail size. It was found that the most unstable CAPE (MUCAPE) had the strongest relation with hail hail size. Moreover, under very weak deep layer shear conditions ($< 5.14$ m/s), there seems to be a linear relation between the maximum possible hail size and MUCAPE. Physically, this can be explained by the fact that the maximum possible hail size is achieved when the terminal velocity equals the maximum updraft velocity. According to the simple parcel theory, the maximum updraft velocity is directly related to the amount of MUCAPE.

# Contents

# 1 Introduction

The occurrence of (severe) hailstorms is relatively rare in the Netherlands. Nevertheless, on the 23rd of June 2016 a extremely severe hailstorm hit the South East of the Netherlands, causing over 500 million euros of damage to houses, cars and agricultural properties (source: Verbond van Verzekeraars). This event was by far the most damaging severe weather event in the last 15 years in the Netherlands. Therefore, there is an increasing demand of a hail detection and forecasting system at the Royal Netherlands Meteorological Institute (KNMI) for nowcasting purposes and, ideally, warning the society when conditions are favorable for severe thunderstorms. Also, insurance companies can use a hail detection system for verification of insurance claims. To create such a hail detection system, Hail Detection Algorithms (HDAs) are used. HDAs use radar data in combination with several other parameters such as temperature profile, cloud top temperature or the height of a certain reflectivity value. The output of HDAs range between indicating whether it is possible hail occurs with certain conditions [Auer Jr., 1994] to an indication of hail size [Witt et al., 1998]. In the second part of the thesis, a climatology is made by applying a HDA to historical data. This is already done for, among others, the United States [Cintineo et al., 2012] and Germany [Junghänel et al., 2016], but currently no climatology of large hail exists for the Netherlands. The last part of this thesis focuses on creating a hail size forecasting method. Several attempts have been done to create such a forecasting method. For example, Miller [1972] created a method based on the buoyancy measured between the LCL (Lifted Condensation Level), the -5°C level and the freezing level. Jewell and Brimelow [2009] created a coupled hail and cloud model called 'HAILCAST'. Even though Jewell and Brimelow [2009] noted that the output of this model is reliable and does not calculate unrealistically high values of hail size during high CAPE and/or vertical wind shear, this model is relatively complicated. During the last part of this thesis, multiple parameters and hail forecast methods found in literature are compared. The outcomes of the analysis leads to a fairly simple hail forecasting method which can easily be implemented at the KNMI (or other institutions) for operational purposes.

# 2 Data

In contrast to rain, hail is currently not measured by automatic weather stations. Besides, due to the very local nature of a storm, hail will most probably miss most of the weather stations. Therefore it is very hard to see where hail events occurred. The ESSL (European Severe Storm Laboratory) created a database in which amateur meteorologists can submit severe weather reports. The amount of people who submit severe weather reports to the European Severe Weather Database (ESWD) is growing, but the size of the database for storms within the Netherlands is still small. Besides, the observations are often made when a storm passes through populated areas. The database does not have many observations in rural areas due to the small population density. For these reasons it is not possible to use these observations for creating a large hail climatology and a hail forecast system. Weather radars however, can cover a vast area with a regular sampling frequency. It is possible for radar to detect precipitation for every square kilometer. Therefore, several attempts have been made to detect (large) hail with the use of Hail Detection Algorithms (HDAs). HDAs make use of radar, and sometimes also temperature soundings (either measured by radiosondes or derived from Numerical Weather Prediction (NWP) models). Details of the HDAs can be found in section 3. In the following section, it is explained which radars are used. Also, a physical explanation of the weather radar is provided. Finally, the section describes methods used to prepare the radar data for use in the HDAs and some difficulties arising when using radar data.

## 2.1 Observations

### 2.1.1 Reports

Even though the observations can not be used for creating a large hail climatology or forecast system, it can be of further use in this thesis. According to the technical report of the ESSL [Groenemeijer et al., 2011], hail is reported to the ESWD when the hailstones have a diameter of 2.0 cm or more, or smaller hailstones that form a layer of 2.0 cm or more on flat parts. The ESWD maintain several quality checks for the reports. A report with quality check 0 (QC0) is marked 'as received', meaning that the quality of the observation still has to be verified. Quality check 1 (QC1) is marked 'confirmed by reliable source', but still some aspects of the report are under discussion. Quality check 2 (QC2) is marked as 'fully verified'. More information about reports submitted to the ESWD can be found in the Technical report 2011-01 [Groenemeijer et al., 2011].

### 2.1.2 Radar

In the Netherlands, two identical single-polarization Meteor 360AC C-band Doppler weather radars offer complete coverage of the Netherlands [Beekhuis and Holleman, 2010]. The radar towers are located in De Bilt (5.17834E, 51.10168N, WGS-84) and Den Helder (4.78997E, 52.95334N, WGS-84). The locations are highlighted in figure 1a. These radar towers transmit highly energetic, short pulses of electromagnetic energy. The wavelengths of these pulses are in the range between 4 cm and 8 cm (C-band). Since this is often much larger than the size of the particles measured, Rayleigh scattering causes a part of the electromagnetic pulse to be backscattered. Another part of the radar is the receiver. This device measures the reflected signal and transforms this signal into a measure of reflectivity according to the (simplified) Probert-Jones equation [Probert-Jones, 1962]:

$$Z = \frac{P_r R^2}{C_r L_a} \tag{1}$$

where $Z$ is in $\mathrm{mm^6 m^{-3}}$,$P_r$ is the amount of power returned to the radar in Watts, $R$ is the distance to the radar, $C_r$ is a radar constant and $L_a$ is the attenuation factor.

The reflected signal is related to the amount of particles per unit volume ($n_i$) and the particle diameter $D_i$ [Battan, 1973] according to:

$$Z = \sum_i n_i \cdot D_i^6 \tag{2}$$

Since in meteorology, 'dBZ' is a more usual unit to work with, equation 2 can be converted to dBZ according to

$$\mathrm{dBZ} = 10 \log_{10} Z \tag{3}$$

The radars in De Bilt and Den Helder scan at 14 different elevations every 5 minutes. In this way, it is possible to make a vertical profile of the reflectivity. An schematic view of the 14 scans is shown in figure 1b. The altitude of the measured reflectivity of each scan is increasing with distance from the radar tower according the equation defined by Yuter [2003]:

$$h = h_0 - \frac{4}{3}R + \sqrt{r^2 + \frac{4}{3}R^2 + 2r\frac{4}{3}R\sin\phi} \tag{4}$$

where $h_0$ is the height of the radar above the ground, $R$ is the radius of the earth, $r$ is the horizontal distance from the radar and $\phi$ is the angle with respect to the surface (elevation angle). This formula includes both the curvature of the earth and refraction by a standard atmosphere [Yuter, 2003]. The maximum range of the radar signal ranges from 320 kilometers at small elevations to 120 kilometers at large elevations. Table 1 shows the different scan numbers with their elevations, radial velocity of scanning, maximum range and the bin size.

## 2.2 Preparing reflectivity data

The reflectivity data from both radars is stored in separate HDF5 format files. The KNMI stores one HDF5 file containing reflectivity data every five minutes for one radar. To create 3D reflectivity data covering the Netherlands, the data is loaded into a 3-dimensional Python array using the Python package 'h5py'. This 3-dimensional array contains the azimuth ($\theta$), distance from the radar ($r$) and the scan number ($n$). Since polar coordinates are not preferable for combining radar data with NWP model data, the reflectivity data must be converted to Cartesian coordinates. This is done by predefining an empty 3-dimensional array (x,y,z). The physical size of the array is 500x500x20 km with $\Delta$x=1 km, $\Delta$y=1 km and $\Delta$z=200 m. First, it is determined which grid cells are associated with the location of a radar tower. This is where the center of the polar grid is located. A computer algorithm now goes through all Cartesian grid cells individually and calculates the direct distance to the radar position according to

$$r = \sqrt{x^2 + y^2} \tag{5}$$

The angle (azimuth) with respect to the radar tower is now calculated according to

$$\theta = \frac{\arctan\left(\frac{x}{y}\right)}{\pi \cdot 180^\circ} \tag{6}$$

Next, the values of r and theta are used to lookup the corresponding reflectivity value for every x, y and z. When this is done for both radar towers, the two cubic grids are put together to form one 3D grid containing reflectivity data from both Den Helder and De Bilt radar towers. The amount of measurements in the vertical is limited (at maximum 28, but in practice this is much less) compared to the 100 grid cells available in the vertical. To make a continuous vertical profile of the reflectivity, the data is interpolated over the vertical resulting in a vertical profile with a minimum height of 100 m and a maximum height of 20 km (dz=200 m). More about interpolation of the vertical reflectivity profile can be found in section 4.1.

**Important assumptions/notes**

1. At locations where no data is available (where the grid cell contains 'NaN' values), the reflectivity value for that grid cell is set to 0 dBZ. This is done for computational purposes, since some Python packages used are not compatible with NaN values.
2. Reflectivity values below 0 dBZ are set to 0.1 dBZ. The value 0.1 is deliberately chosen such that it distinguishes from the NaN values.
3. The radius of the earth is assumed to be 6371 km
4. It is assumed that both radars are located 30 meters above ground.
5. Altough the beam width is about 1 degrees, only the line which denotes the middle of the beam is taken into account.

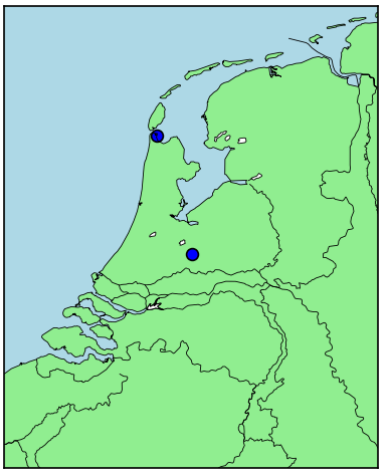

(a) Map showing the locations of both radar towers

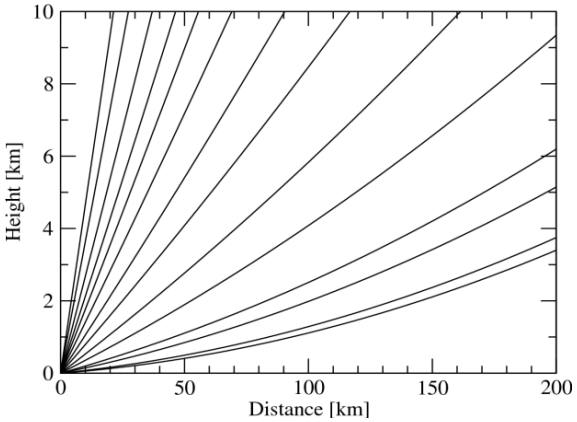


(b) Graph illustrating 14 scans and their propagation in height with increasing distance from the radar according to equation 4

Figure 1

Table 1: Parameters for the volume radar scan

| Number | Elevation (deg) | Deg/sec | Range (km) | Binsize |
|---|---|---|---|---|
| 1 | 0.3 | 18 | 320 | 1.0 |
| 2 | 0.4 | 18 | 240 | 1.0 |
| 3 | 0.8 | 18 | 240 | 1.0 |
| 4 | 1.1 | 18 | 240 | 1.0 |
| 5 | 2 | 18 | 240 | 1.0 |
| 6 | 3 | 24 | 170 | 0.5 |
| 7 | 4.5 | 24 | 170 | 0.5 |
| 8 | 6 | 30 | 145 | 0.5 |
| 9 | 8 | 30 | 145 | 0.5 |
| 10 | 10 | 30 | 120 | 0.5 |
| 11 | 12 | 36 | 120 | 0.5 |
| 12 | 15 | 36 | 120 | 0.5 |
| 13 | 20 | 36 | 120 | 0.5 |
| 14 | 25 | 36 | 120 | 0.5 |

## 2.3 HIRLAM

Some HDAs make use of vertical temperature profiles. At the time the HDAs were developed, the temperature profiles were provided by radiosonde measurements. Nowadays, NWP models are used because less radiosondes are available. In this thesis, the weather model HIRLAM (High Resolution Limited Area Model) version D11 is used which has a horizontal resolution of 11 km and contains 60 vertical levels[1] ranging between the surface and 10 hPa. The forecasting time range of HIRLAM D11 is +48 hours and the achieved 3D data has a time resolution of 3 hours. In table 2 an overview is shown of the runs used in this research. Since it is a limited area model,

Table 2: HIRLAM runs used per the time window of interest

| Time window | HIRLAM run |
|---|---|
| 0:00 UTC - 2:55 UTC | D11 0:00 +3 |
| 3:00 UTC - 5:55 UTC | D11 0:00 +3 |
| 6:00 UTC - 8:55 UTC | D11 0:00 +6 |
| 9:00 UTC - 11:55 UTC | D11 6:00 +3 |
| 12:00 UTC - 14:55 UTC | D11 6:00 +6 |
| 15:00 UTC - 17:55 UTC | D11 12:00 +3 |
| 18:00 UTC - 20:55 UTC | D11 12:00 +6 |
| 21:00 UTC - 23:55 UTC | D11 18:00 +3 |

it only covers a part of the total atmosphere. Figure 2a shows the total domain of the HIRLAM D11 model. The lateral boundary conditions are provided by the ECMWF (European Center for Medium range Weather Forecast) model. To combine HIRLAM data with data from the radar, the data is first converted to grids in regular lat/lon coordinates, instead of the rotated grid shown in figure 2a. The standard data format in which HIRLAM data is stored is 'GRIB'. These GRIB

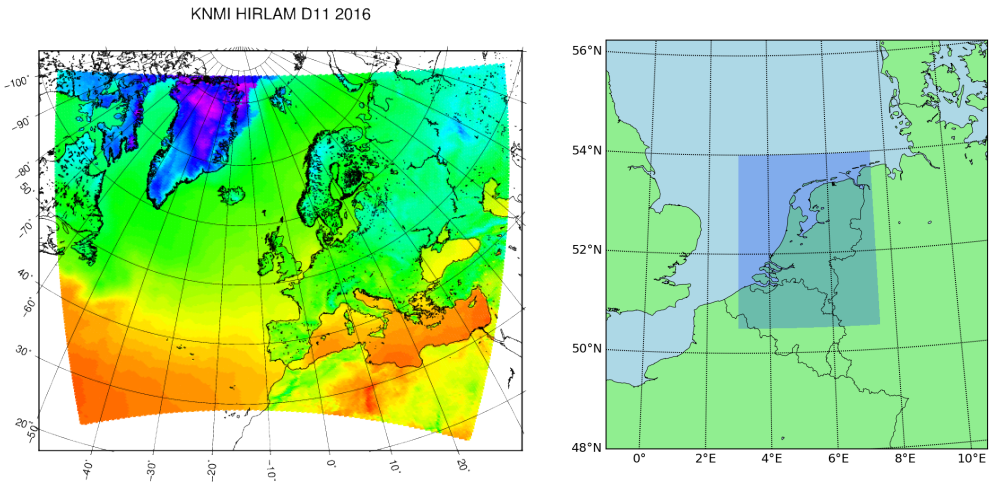


(a) Map highlighting the total HIRLAM D11 domain on a rotated grid

(b) Map highlighting the domain of interest for this thesis

Figure 2

files are modified such that only the domain of interest remains (figure 2b), which ranges between longitudes of 3°E-7.5°E and latitudes 50.5°N-54°N. The GRIB files are loaded into a Python program with the use of the Python package 'pygrib'. Using this package, it is possible to load temperature data for every vertical level provided by HIRLAM into a 3-dimensional array with the same vertical resolution as the array in which the radar data is stored. Since these levels are dynamic (e.g. obtained from a geopotential surface), the height above sea level can be calculated

[1] HIRLAM contained 40 vertical levels before 2010

by

$$z = \frac{\Phi}{g} \tag{7}$$

where $\Phi$ is the geopotential height (also obtained from the HIRLAM weather model) and $g$ is the gravitational acceleration (9.81 $\mathrm{ms}^{-2}$). To create a vertical temperature profile, the 60 levels[2] have to be interpolated linearly to 100 levels as the 3-dimensional array prescribes. Since the horizontal resolution of HIRLAM is much lower than that of the radar, the resolution of the HIRLAM data is increased to 1x1 km using the function 'imresize' from the 'SciPy' python package.

[2]For the HIRLAM datasets 2008 and 2009, only 40 dynamic levels are available. These 40 levels are interpolated in the same way as described for the other datasets

# 3 Hail Detection Algorithms (HDAs)

In this section the most important and most widely used HDA's are discussed to give an indication of different methods used by researchers to distinguish between hail and rain. Eventually, one of these algorithms is chosen to use for further analysis in this thesis.

## 3.1 Waldvogel et al. [1979]

For the purpose of hail suppression, Waldvogel et al. [1979] developed a fairly simple technique which is a combination between thermodynamic sounding and radar data. For this algorithm, the height of the freezing level ($H_0$) and the height of the 45dBZ echo ($H_{45}$) are compared. Using empirically determined lookup tables, Waldvogel et al. [1979] determined the probability for the occurrence of hail. This method combines an indicator for very strong updraft speeds (e.g. the height of the 45 dBZ reflectivity core) with the presence of large amounts of undercooled water (the strong 45 dBZ reflectivity core).

## 3.2 Auer Jr. [1994]

The HDA developed by Auer Jr. [1994] uses CAPPI (Constant Altitude Plan Position Indicator) reflectivity in combination with cloud top temperatures. The term 'CAPPI' means that the radar data is shown at a constant altitude. The cloud top temperatures are obtained by geostationary satellites such as Meteosat measuring infrared radiance [Holleman, 2001]. Auer Jr. [1994] found a differentiation between hail and no hail (rain) evens by using over 100 hail or rain cases in New Zealand. It was found that there is a reflectivity threshold below which no hail occurred. This threshold is found to be lower for higher cloud top temperatures and vice versa according to:

$$Z_{Th} = \begin{cases} -0.38 \cdot (T_{top} - 85.0) & T_{top} \leq -11°C \\ 1.33 \cdot (T_{top} + 38.8) & T_{top} > -11°C \end{cases} \tag{8}$$

When assuming rainfall rate to be related according to the Marshall-Palmer relation:

$$Z = 200R^{1.6} \tag{9}$$

very high reflectivity values of about 60 dBZ correspond to rainfall rates of about 205 mm $h^{-1}$. Since these rainfall intensities are extremely rare, the reflectivity threshold made by Auer Jr. [1994] corrects for these high reflectivity values by marking these reflectivities as being hail.

## 3.3 Amburn and Wolf [1997]

Greene and Clark [1972] stated that the concentration of liquid water in clouds is of considerable meteorological importance. They proposed a relationship which connects radar reflectivity to liquid water content (LWC). Mathematically, the liquid water content per unit volume can be described as

$$M = \frac{\rho_w \pi}{6} \int_0^{a_{max}} n(a) a^3 da \tag{10}$$

Where M is in g $m^{-3}$, $\rho_w$ is the density of water and $n(a)$ is the amount of water droplets with diameter $a$, where $a$ is in meters. Combining equation 10 with equation 2 yields

$$M = 3.44 \times 10^{-3} Z^{4/7} \tag{11}$$

where Z is the reflectivity in $mm^6 m^{-3}$. Integration over height results in the Vertically Integrated Liquid water (VIL):

$$\text{VIL} = \int_{h_b}^{h_t} M dh \tag{12}$$

where the VIL is in $kgm^{-2}$, $h_t$ is the cloud top and $h_b$ is the cloud base. This algorithm is based on the assumption that the vertically integrated column consists solely of liquid water. Obviously, this is not the case during large hail events. However, under influence of large hail, very high values of the VIL will be returned. Greene and Clark [1972] stated that these very high values of the VIL

can be indicative for the severity of a storm. Amburn and Wolf [1997] stated however, that the VIL value in the case of large hail events varies greatly with severe hail ground reports because of the differences in airmass characteristics resulting in different kinds of hydrometeors. Different hydrometeors have significantly different reflectivity characteristics and therefore the VIL alone is not a very good estimation of the amount of hail or hail size in a certain thunderstorm. A possible solution for this is assigning a 'VIL of the day'. This value of the VIL is used as a threshold value below which is assumed no severe thunderstorms will occur. This value is based on the the temperature profile. Several attempts have been done in order to obtain a good value for the VIL of the day but Amburn and Wolf [1997] noticed some disadvantages. First of all, when determining the VIL of the day one has assumed that the state of the atmosphere is uniform within the range of the radar, which clearly is not necessarily the case. Another problem with the definition of VIL is that small, shortlived thunderstorms with high reflectivity values may produce the same VIL value as tall, longlived thunderstorms with low reflectivity values. Even though the smaller thunderstorm could have produced large hail and the larger thunderstorm did not, the VIL values will be the same. This clearly is problematic when evaluating large hail events. Amburn and Wolf [1997] therefore proposed the VIL density. This value of the VIL is normalized with respect to the height of the storm cell. In this way, it is possible to quickly identify thunderstorms with high reflectivities with respect to the height. The VIL-density is defined as

$$\mathrm{VIL_{density}} = \mathrm{VIL}/\mathrm{Z_{top}} \tag{13}$$

where the the VIL density is in g $\mathrm{m}^{-3}$ and the echotop ($Z_{top}$) is defined as the highest level where reflectivity values exceed 20 dBZ. Although the VIL density will increase when the thunderstorms increase in height, the VIL density primarily increases due to the increase in target size. It turns out that the VIL density shows some correlation with reports of hail size on the ground. Amburn and Wolf [1997] did not give a detailed statistical analysis, but nevertheless they stated that they correctly identified 90% of the severe hail cases using a VIL-density threshold of 3.5 g $\mathrm{m}^{-3}$.

## 3.4 Witt et al. [1998]

In order to determine the size of hail, an attempt has been done by Witt et al. [1998] to improve the VIL algorithm made by Amburn and Wolf [1997]. They make use of a cell-base algorithm called SCIT (Storm Cell Identification and Tracking Algorithm) [Johnson et al., 1998]. This is different from the grid-based algorithm used to determine VIL and VIL-density. The SCIT algorithm is not going to be used, as it is beyond the scope of this thesis. The second improvement involves the assumption that that the hail kinetic energy ($\dot{E}$) is related to the reflectivity, shown by Waldvogel et al. [1978]. In their research, they measure the amount and size of hail stones that fall at a predefined surface during a predefined time window. They calculated the hail kinetic energy according to

$$\dot{E} = \frac{\pi \rho v_0^2}{Ft(12 \times 10^6)} \sum_{i=0}^{p} n_i D_i^4. \tag{14}$$

Where $\rho$ is the density of the hailstone, $v_0 = 4.41\mathrm{m}^{-1}\mathrm{mm}^{-0.5}$, $F$ is the sampling area and $t$ is the sampling time. The parameter $n_i$ represents the number of hailstones in the diameter interval $D_i \pm \frac{1}{2}\Delta D_i$ (more about the intervals can be found in Federer and Waldvogel [1975]). Waldvogel et al. [1978] now calculated the corresponding reflectivity in a similar way since, as shown in equation 2, the reflectivity and amount of particles with diameter D per unit volume are related. They ultimately found an empirical relationship between the hail kinetic energy and the reflectivity defined as:

$$\dot{E}(Z) = 5 \cdot 10^{-6} \cdot 10^{0.084Z} \tag{15}$$

where $\dot{E}(Z)$ is in $\mathrm{Jm}^{-2}\mathrm{s}^{-1}$ and $Z$ is in dBZ. Witt et al. [1998] uses an adapted version of equation 15:

$$\dot{E}(Z) = 5 \cdot 10^{-6} \cdot 10^{0.084Z} W(Z) \tag{16}$$

where

$$W(Z) = \begin{cases} 0 & Z \leq Z_L \\ \frac{Z - Z_L}{Z_U - Z_L} & Z_L < Z < Z_L \\ 1 & Z \geq Z_U \end{cases} \tag{17}$$

In this thesis $Z_L = 40$ dBZ and $Z_U = 50$ dBZ, which are the same values used by Witt et al. [1998] but it is stated that these values are adaptable. From equation 17 it can be seen that this weighting function filters out lower reflectivity values and focuses on higher reflectivity values which are related to hail. A second weighting function is introduced which is based on the vertical temperature profile:

$$W_T(H) = \begin{cases} 0 & H \leq H_0 \\ \frac{H-H_0}{H_{m20}-H_0} & H_0 < H < H_{m20} \\ 1 & H \geq H_{m20} \end{cases} \tag{18}$$

where $H$ is the height above the radar level, $H_0$ is the freezing level and $H_{m20}$ is the level at which the temperature is -20°C. This weighting function is introduced since hail will not form below the freezing level. Temperatures lower than -20°C are ideal for creating hail and therefore this weighting function will have the value 1 above the -20°C-level. Between the -20°C-level and the freezing level, the value of $W_T$ will be between 0 and 1, depending on the height. In this thesis, NWP model data from HIRLAM is used for determining the temperature profile. Combining all of the above, leads to the Severe Hail Index (SHI) defined by Witt et al. [1998]:

$$\text{SHI} = 0.1 \int_{H_0}^{H_40} W_T(H)\dot{E}dH \tag{19}$$

where $H_40$ is the 40 dBZ echotop. The SHI is in $\text{Jm}^{-1}\text{s}^{-1}$. Witt et al. [1998] used statistical analyses to find that the optimum warning threshold for large hail was linearly correlated to the freezing level ($H_0$). From this they obtained a Warning Threshold Selection Model (WT) defined as

$$\text{WT} = 57.5H_0 - 121 \tag{20}$$

This forms the basis for a probability function for the occurrence of large hail:

$$\text{POSH} = 29 \ln\left(\frac{\text{SHI}}{\text{WT}}\right) + 50, \tag{21}$$

where POSH is the probability of severe hail in %. Negative POSH values are set to 0% and to avoid an unrealistic degree of accuracy, values are rounded off to the nearest 10%.

To give more information about the size of the hail, Witt et al. [1998] compared observed hail sizes with the SHI. They found that the SHI and **maximum** hail size are related according to the fairly simple equation

$$\text{MEHS} = 2.54(\text{SHI})^{0.5} \tag{22}$$

where MEHS is the Maximum Expected Hail Size in millimeters. Since this equation indicates the maximum expected hail size, most of the hail stones will be smaller than the MEHS by definition. Witt et al. [1998] decided that 75% of the observations have to be smaller than the MEHS (figure 3). That means that 25% of the observations are larger than the MEHS. Note that the MEHS is quite arbitrary and can be adapted to make sure all observations are smaller than the MEHS.

## 3.5 Selecting HDA

Witt et al. [1998] discussed the improvement of the new HDA with respect to the 'older' VIL and VIL-density as indicators for hail size (section 3.4). They concluded that indeed there was improvement in indicating maximum hail size. Furthermore, the methods of Waldvogel et al. [1979] and Auer Jr. [1994] do not produce indicators of hail size, which is an essential parameter in this thesis. Even though Witt et al. [1998] noted that the MEHS is sometimes not correct, it does give a good relative hail size indication. It is therefore decided that in this thesis, the HDA made by Witt et al. [1998] is used.

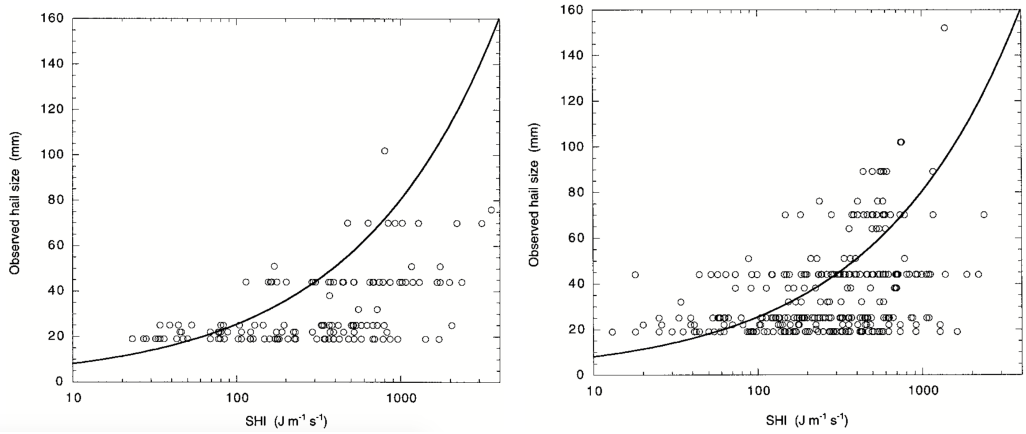


Figure 3: Scatter plot of the SHI vs observed hail size for 147 (left) and 314 (right) hail reports in the United States for 9 and 30 storm days, respectively (figures adapted from Witt et al. [1998])

# 4 Applying the HDA

To apply the HDA by Witt et al. [1998], a Python program was made to import the reflectivity data from both radars into a 3D Python array using the method described in section 2.2. Another script was run to load the temperature profile from HIRLAM files as described in section 2.3. The program then goes through every 3D grid cell and determines the kinetic energy of hail (according to equation 16 and applying the weighting functions). This section describes how a vertical reflectivity profile is created to eventually calculate the SHI. The difference between the cell-based and grid-based methods to calculate the SHI can have some influence on the outcome when a storm is tilted. An attempt has been made in this section to try to correct for this tilt. Finally, a ground clutter filter is developed and described.

## 4.1 Different approaches in determining the vertical profile

The HDA by Witt et al. [1998] makes use of so-called 2D storm components, which are quasi-horizontal cross sections for each elevation angle scanning through the storm cell detected by the SCIT. This is then used to create a vertical reflectivity profile. Witt et al. [1998] state that 'the height and maximum reflectivity of each storm component are used to create a vertical reflectivity profile for the cell'. However, they do not mention exactly how the vertical reflectivity profile is vertically integrated (e.g. interpolation techniques etc.), while this can be of great importance when integrating the reflectivity profile. For this reason, different interpolation methods are used to assess the performance of each of the methods.

### Nearest neighbour

The nearest neighbor interpolation technique propagates vertically and for every 200 meters (which is the spatial step used for the vertical profile in this thesis) the method determines at which height the sampled reflectivity is closest to the current height. This sampled reflectivity is then used for this height until another sample reflectivity is closer to the current height.

### Linear

The linear interpolation technique is straightforward linear interpolation between all the points in the vertical.

### Zero hold

The zero hold interpolation method propagates vertically. When it encounters a sample reflectivity, this value is used until another sample is encountered and so on. Mathematically this can be described as

$$\mathrm{dBZ}(h) = \begin{cases} X_{h-1} & X_h = \mathrm{NaN} \\ X_h & X_h \neq \mathrm{NaN} \end{cases} \tag{23}$$

Where h is the height level and $X$ is the sampled reflectivity.

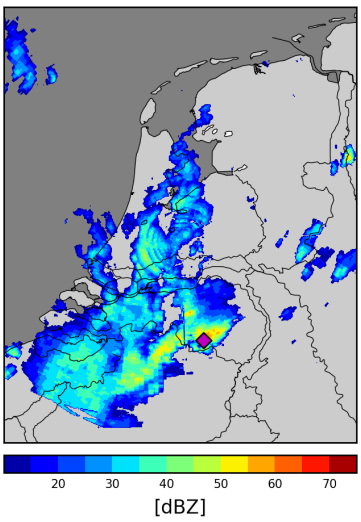


(a) Reflectivity (CAPPI view) at 2km height on 23rd of June 2016 18:35 UTC. The location of the vertical profile is highlighted with the magenta diamond

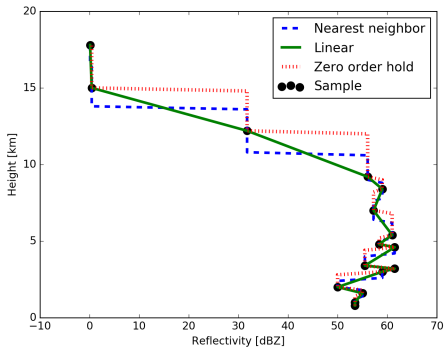


(b) Vertical profile of the reflectivity at the location highlighted in (a), where the different interpolation methods are shown

Figure 4

### 4.1.1 Evaluation

Looking at the different interpolation methods (figure 4b), the linear and nearest neighbor method end up with the same value when integrated. However, because of the weighting functions in the HDA which depend on temperature and reflectivity, these two interpolation methods can result in different outcomes in the HDA. The zero order hold method underestimates the reflectivity with respect to linear and nearest neighbor where

$$\frac{dZ}{dh} > 0 \tag{24}$$

(where $Z$ is the reflectivity in dBZ). The method overestimates the reflectivity where

$$\frac{dZ}{dh} < 0 \tag{25}$$

For these three methods, a small statistical analysis is done in which the observations provided by the ESWD are compared with the outcomes of the HDA for different days. The MEHS is calculated around the same time each ESWD observation was made with a time window of 30 minutes. From 15 minutes before the observation until 15 minutes after the observation the HDA is calculated. The maximum value calculated in this time window is used for the comparison. The outcomes are put into a scatter plot shown in figure 5. According to the statistical analysis, the zero order hold interpolation method has the smallest correlation coefficient and also overestimates the hail size (slope of 0.39). The linear and nearest neighbor method both have higher correlation coefficient and steeper slopes.

Unfortunately, there is low confidence in trying to determine a proper interpolation method according to this statistical analysis because of the low correlation coefficients. These low correlation coefficients probably arise because the observed hail sizes are categorized in bins of 1 cm, therefore rounding off the true hail size. Also, the number of observations is small, making the dataset more sensitive to errors. Having in mind that Witt et al. [1998] stated that they take the maximum

reflectivity value per storm component (which is also done in the nearest neighbor method) it has been chosen to use the nearest neighbor method for further analysis in this thesis.

## 4.2 Tilting of the storm

The SCIT algorithm used in the HDA by Witt et al. [1998] identifies a storm cell and determines the vertical and horizontal extent, effectively creating a 3D grid box which includes all the maximum reflectivity values measured in this grid box. As stated in section 3, the SCIT algorithm is not implemented in this thesis and the grid-based algorithm is used instead. Witt et al. [1998] stated that the disadvantage of the grid-based method is that when the hail core is crossing a grid boundary (e.g. when the storm is tilted), it leads to an incorrect decrease in the SHI. The advantage of the grid based method is, however, that it is less error sensitive than the cell based method. When an error occurs somewhere in a cell, this error will be visible for the whole cell. To compensate for the error which can occur due to the tilt in the storm, the HDA is applied for different grid sizes (4x4km, 8x8km and 15x15km). Thereby decreasing the probability that the hail core will be located across a grid boundary. Another, more sophisticated method used to overcome this problem is proposed by Stumpf et al. [2004]. They tried to correct for tilted storms by using morphological dilation. In this thesis, it is performed on all the 2D reflectivity surfaces (100 in total). The dilation is applied by passing a 5x5 pixel kernel over every data point, in which this data point is replaced by the largest value inside this 5x5 pixel kernel. To decrease the effect of increasing the reflectivity values in the neighborhood around reflectivity maxima, at least 9 of 25 pixels in the kernel should contain non-zero values. Otherwise, zero is returned. A visualization of the morphological dilation can be found in appendix B.

### 4.2.1 Evaluation

Several methods are used for correcting for tilted storms. However, because of the uncertainty in the original HDA output by Witt et al. [1998], it is unnecessary to correct for tilted storms since these corrections only have minor effects on the maximum hail size within a cell (appendix B). Secondly, the number of observations are quite limited and therefore can not provide concluding evidence that the HDA is improved for tilted storms. It is therefore decided that no method for correcting for tilt of the storm is applied in this thesis. Nevertheless, the methods can be of use in research when more observations are available.

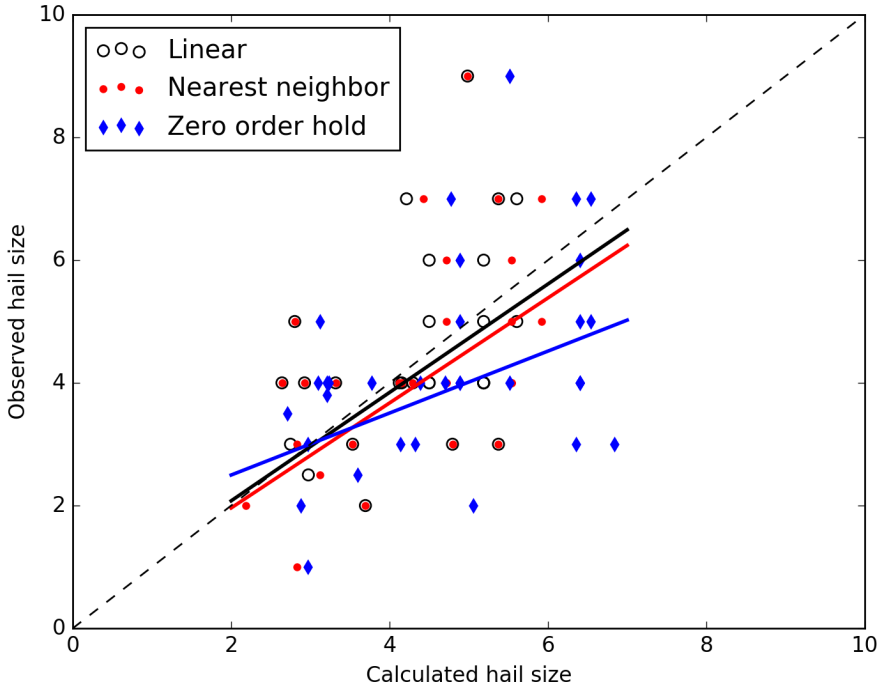


Figure 5: Comparison of the observed hail size with the calculated hail size in cm with the HDA by Witt et al. [1998]. The 36 observed hail sizes are provided by the ESWD with quality check 1 (QC1). The legend shows the colors of the different interpolation techniques used. The lines are polynomial fits and the dashed line is a perfect fit (slope=1).

| Method | r | Slope |
|---|---|---|
| Linear | 0.38 | 0.83 |
| Nearest neighbor | 0.36 | 0.71 |
| Zero order hold | 0.23 | 0.39 |

Table 3: Statistical parameters for the polynomial fit shown in figure 5

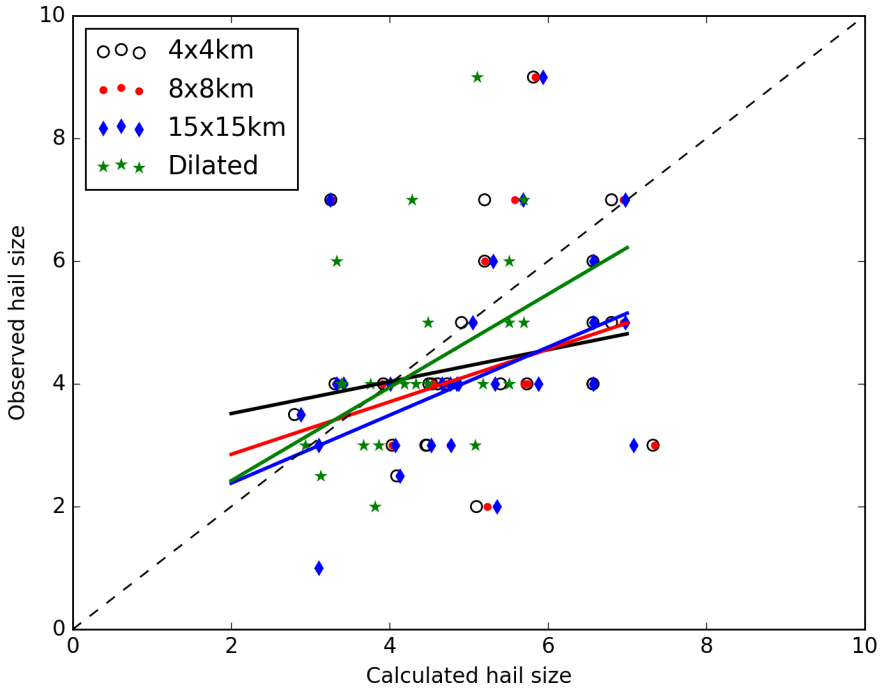


Figure 6: Same as in figure 5. The legend shows the different techniques to deal with tilting of the storm.

| Method | r | Slope |
|---|---|---|
| 4x4km grid | 0.17 | 0.26 |
| 8x8km grid | 0.28 | 0.43 |
| 15x15km grid | 0.37 | 0.55 |
| Dilation | 0.37 | 0.76 |

Table 4: Statistical parameters for the polynomial fit shown in figure 6

## 4.3 Ground clutter

It was observed that on some days the radar reflectivity has an unnatural spatial pattern, often during nighttime. At night, a temperature inversion is often present, leading to a very strong decrease in density with increasing height. Since a radar beam is emitted with a very small angle with respect to the lines of constant density, the radar beam is refracted downwards under influence of the stratification, deviating from the expected beam height (equation 4). Eventually, the radar beam reflects off buildings, wind turbines or other structures at the earth's surface. Because of the deviation from the expected height, reflectivity signals relatively far away from the radar tower (at least 100 km) are incorrectly analyzed as being on some height above ground. The visible effect is called 'ground clutter'. In order to make a climatology, it is unacceptable to have ground clutter in the dataset. Therefore, an attempt has been made to filter out ground clutter.

It has been observed that at locations where ground clutter is present, the vertical reflectivity profile does not have a consistent pattern because some scans do not experience the effect causing ground clutter. Actual storm cells do not have this inconsistency in their vertical profiles (figure 7). The inconsistency can be indicated by variance ($\sigma^2$) in the vertical reflectivity profile as:

$$\sigma^2 = \frac{1}{N}\sum_{i=1}^{N}(Z_i - \mu)^2 \tag{26}$$

where N is the amount of steps in the vertical profile (in this case 100 steps), $Z$ is the reflectivity in dBZ and $\mu$ is the average reflectivity value in the vertical profile in dBZ. The variance is now calculated for every grid cell. Every grid cell where the radar has measured 6 or more reflectivity values and $\sigma^2 > 140$ between 2000m and 8000m, the value of this grid cell is set to zero. These values were obtained by trial and error. Results (figure 28 in appendix A) of the analysis[3] show that a large part of the ground clutter is filtered out. A possibility exists that parts of a real storm cell are filtered out. However, it is observed that this only happens with lower values of the reflectivity and thus this filtering technique does not have a significant effect on MEHS larger than 2 cm (figure 28e and 28f).

### 4.3.1 Evaluation

It has been shown that a relatively simple method can be used as a ground clutter filter. Using this method, most of the false echoes are filtered out. Unfortunately, it does not remove ground clutter at cities far away from the radar (Tilburg and Groningen for example, figure 29a). To overcome this problem it has been chosen to ignore the data obtained from the lowest scan (scan 1 with an elevation of 0.3°) of both radars. Even though the maximum range decreases when ignoring the lowest elevation, nearly all ground clutter within the borders of the Netherlands are filtered out (figure 29).

[3]The filter is applied and eventually the MEHS is calculated. Note that the outcome of the HDA is calculated in a testing phase within this thesis. Therefore, the absolute values of the MEHS in this analysis are incorrect and therefore irrelevant.

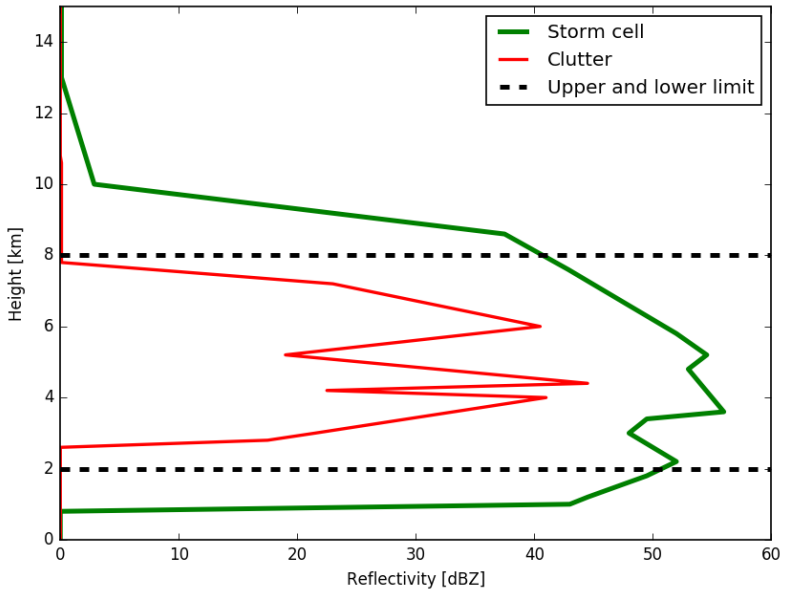


Figure 7: Vertical profile of the reflectivity at a location where an actual storm cell is present (green line) and a location where clutter is present (red line).

# 5 Case study (23 June 2016)

The relevance of this thesis to accurately detect large hail can be shown with the case on the 23rd of June 2016. A supercell in the South East of the Netherlands producing hail with sizes up to 9 cm caused over 500 million euros of damage to roofs, glass houses and cars. Figure 8 shows a glass house which is completely destroyed by the hail. This hailstorm is by far the most damaging severe weather event in the last 15 years. To illustrate, extreme winds corresponding to the mid-latitude depression 'Kyrill' in January 2007 caused about 171 million euros of damage (source: Centrum voor Verzekeringsstatistiek).

## 5.1 Synoptic situation

In the night between the 22nd and 23rd of June, there already were some thunderstorms present near the western coast of the Netherlands. These thunderstorms were triggered by a low pressure system west of Scotland (figure 11), causing advection of very warm and moist air from the South-west of Europe to the Netherlands. This situation continued throughout the 23rd of June (figure 12). Additionally, a so called 'thundery low' developed in western France. A thundery low often forms in the exit region of a mid-tropospheric jet streak under influence of frontogenesis due to the warming of the land and the relatively cool Atlantic ocean [Van Delden, 2000]. Especially in the South East of the Netherlands, very high dew point temperatures were measured (almost 23 °C, which is among the highest ever recorded in the Netherlands). Combined with temperatures of about 32°C, MUCAPE values reached as high as 3500 J/kg (figure 13 and figure 14).

## 5.2 Supercell

Throughout the 23rd of June, temperatures increased steadily and moist air was advected by a southwesterly wind to the Netherlands. At about 15:00 UTC, the wind shear between 0-6 km was as high as 26 m/s and CAPE values about 3000 J/kg (figures 13 and 14). However, no triggering mechanism was present for showers to develop. Later in the day, CAPE values even reached 3500 J/kg and wind shear in these high CAPE regions was about 22 m/s. Due to the passage of an upper tropospheric trough (thundery low) which acted as a triggering mechanism, a supercell was able to develop around 17:30 UTC in the North of Belgium and eventually entered the Netherlands near the town of Luyksgestel around 18:30 UTC. At that moment, the supercell already produced hail of about 7 cm according to reports submitted to the ESWD. The supercell headed Northeast where it produced large hail of about 9 cm near the town of Someren around 18:45 UTC. After

Figure 8: Destroyed glass houses in the town Asten (Photo: Omroep Brabant)

that, the supercell decreased in strength and crossed the Dutch-German border around 19:45 UTC, where it continued to exist for at least 1.5 hours. An overview of all the reports made during the passage of the supercell are shown in figure 10.

## 5.3 HDA applied

It is now interesting to apply the HDA to this specific case. Figure 9 (left) shows a cumulative image of the calculated maximum hail size (MEHS) between 18:00 UTC and 21:00 UTC. Interestingly, the highest value of the MEHS is about 6.5 cm, which is about 2.5 cm smaller than the maximum hail size submitted at the ESWD. Nevertheless, when looking at figure 10 the locations of the reports correspond very well with the calculated hail path. Figure 9 (right) shows the destructive path of the hail storm. This figure shows that there is a quite good potential in applying the HDA for verifying insurance claims for insurance companies.

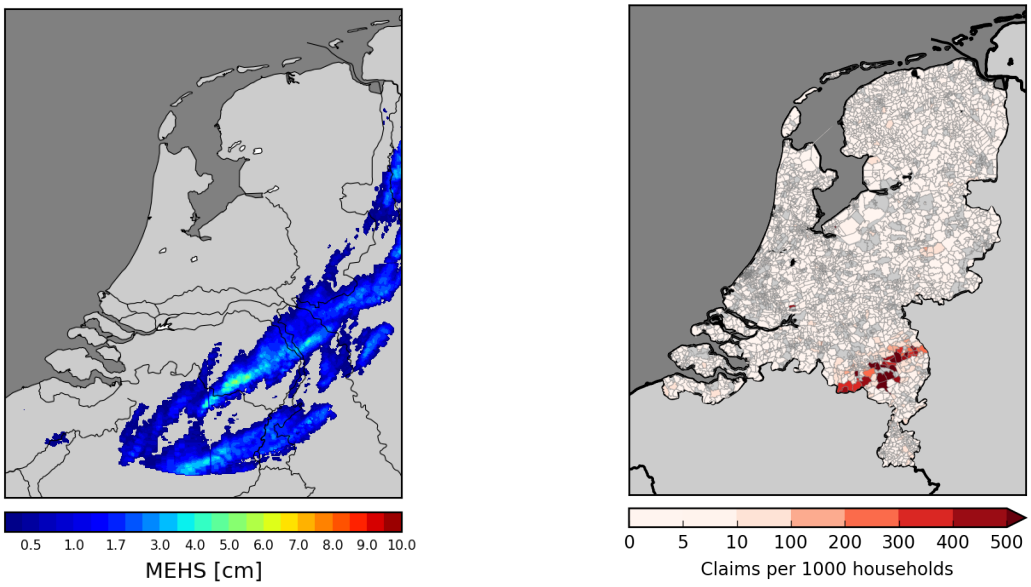


Figure 9: Cumulative image of the MEHS at 23-06-2016 between 18:00 and 21:00 UTC (left) and the corresponding insurance claims per postal code region per 1000 households at the 23rd of June 2016 (right). Data source: Verbond van Verzekeraars.

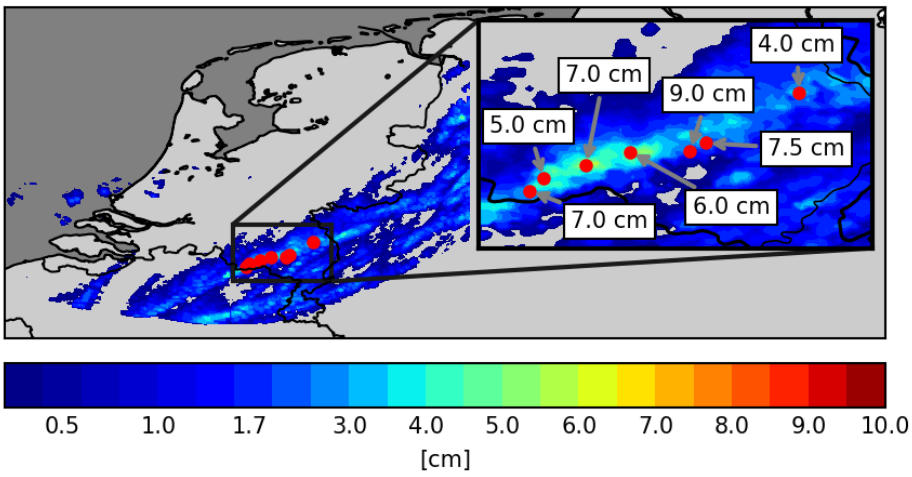


Figure 10: Overview of the ESWD reports made on 23-06-2016. The inset annotates the size of hail that is reported. The colors show the value of the MEHS.

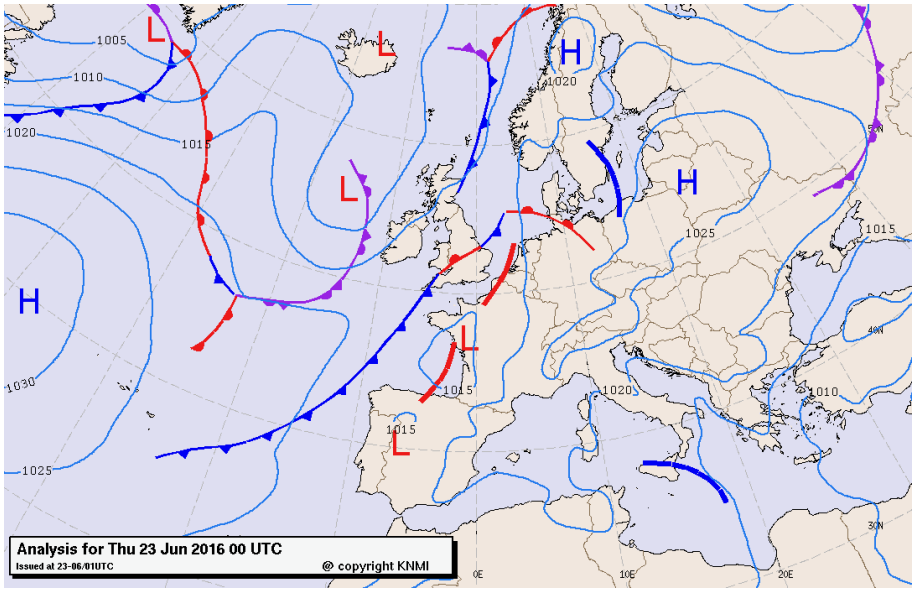


Figure 11: Synoptic situation on the 23nd of June 2016 00:00 UTC

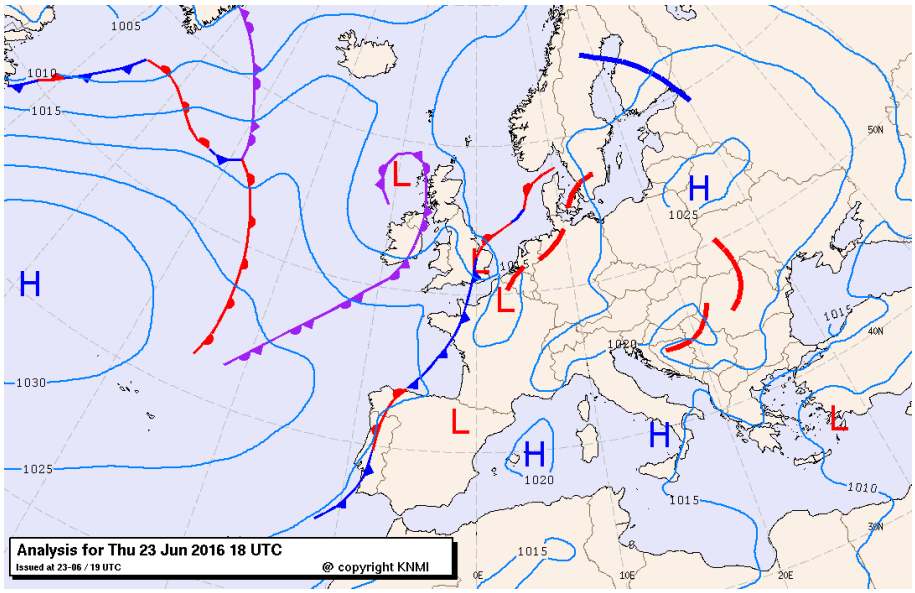


Figure 12: Synoptic situation on the 23rd of June 2016 18:00 UTC

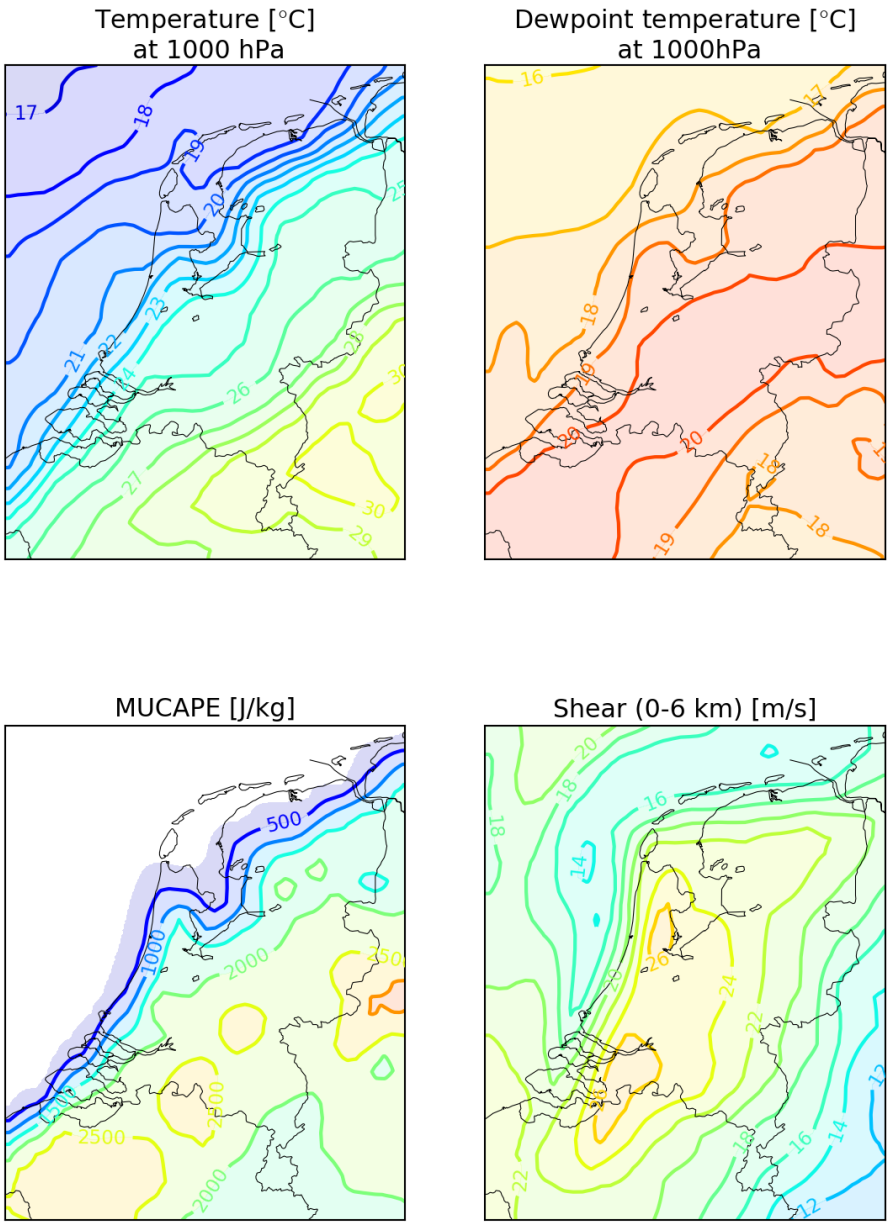


Figure 13: HiRLAM output of run 23-06-2016 12:00 UTC +6 (valid at 18:00 UTC) showing temperature, dewpoint temperature, MUCAPE and shear between 0-6 km.

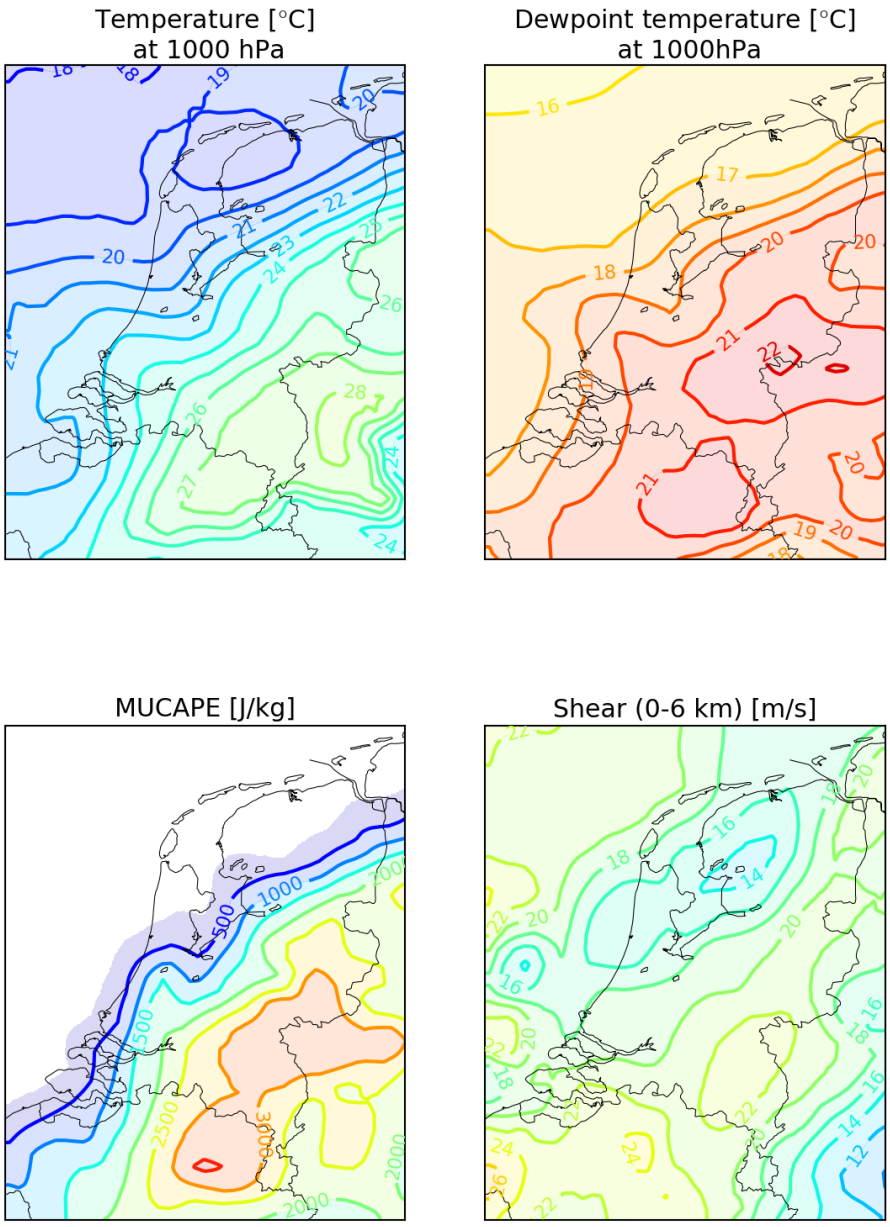


Figure 14: HiRLAM output of run 23-06-2016 18:00 UTC +3 (valid at 21:00 UTC) showing temperature, dewpoint temperature, MUCAPE and shear between 0-6 km.

# 6 Climatology of large hail between 2008 and 2016

The main goal of this thesis was to create a climatology of large hail in the Netherlands. The KNMI stores single polarization volume radar data from 2008 and onwards. Therefore it is only possible to create a climatology between 2008 and 2016.

## 6.1 Date selection

Because applying the HDA to every day since 2008 is very inefficient, it is important to select dates before applying the HDA. Therefore, it is assumed that hailstorms only occur when a large amount of CAPE is present. On the other hand, the CIN (Convective Inhibition) has to be sufficiently small to release convection. The amount of CAPE which has to be present inside the domain has to be at least 1500 $Jkg^{-1}$ and the CIN has to be at least -100 $Jkg^{-1}$. Applying these threshold values results in a selection of 211 days[4], reducing the size of the dataset by 93%.

## 6.2 Observations

Due to the very local nature of a hailstorm and the fact that hail stones melt rapidly when they reach the ground, not many observations of large hail are available. Amateur observers have reported hail events to the ESWD. An overview of all reports can be seen in figure 15. This figure clearly illustrates the very limited nature of large hail observations.

## 6.3 Large hail Climatology

To make a climatology for the Netherlands between 2008 and 2016, a Python program was made to calculate the MEHS and POSH for the selected days at every grid cell at every time step. Secondly, a cumulative file is made which contains the maximum value for the MEHS and POSH for a certain day. Again, all these cumulative files are added together in the same way to create a file which contains the maximum value for the MEHS and POSH for the period 2008 - 2016. The results are shown in figure 17a and 17b. Overall, we see that the occurrence of large hail is rare. Nevertheless, it can be seen that in the South-East of the Netherlands, the largest hail sizes and probabilities for large hail are calculated.

A third climatology product is made which contains the number of occurrences in a certain period. This product is made by calculating the number of days at which the MEHS is larger than 2, 3 or 4cm for every grid cell. The results are shown in figure 18. The results show that the South East of the Netherlands have more large hail days (e.g. days where the MEHS is larger than 2cm) than the North East. This can also be seen in the 3 and 4cm occurrences (Figure 18b and 18c).

In figure 16, the frequency distribution per month is shown. From this analysis, it can be seen that most of the large hail days (85%) occur in June, July and August. This can be a manifestation of the fact that temperatures are highest in these months, therefore leading to high CAPE values. Interestingly, hail sizes larger than 3cm seem to be concentrated in June. Unfortunately, no possible explanation can be found for this observation.

[4]The following selected days are not included in the climatology due to lack of data: 25-08-2009, 09-07-2010, 23-08-2011, 26-08-2011. Also parts of 24-08-2009 and 28-06-2016 suffer from data loss

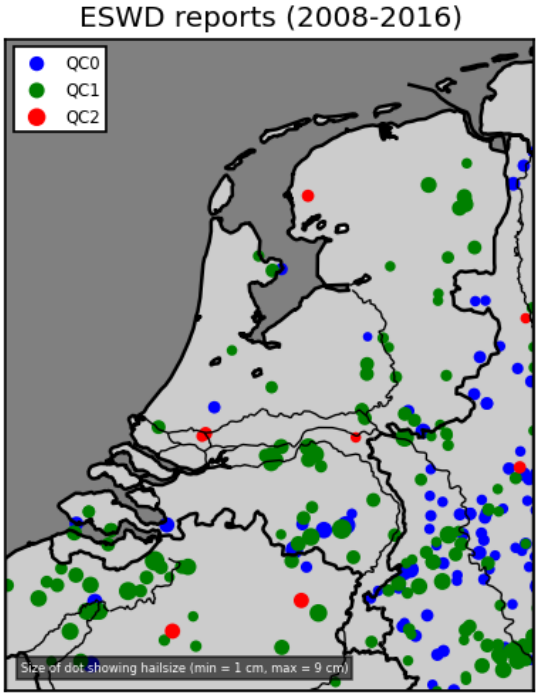


Figure 15: An overview of all large hail reports submitted at the ESWD between 2008 and 2016. The definition of the different quality checks (QC0, QC1 and QC2) can be found in section 2.1. The size of the dot indicates the reported hail size.

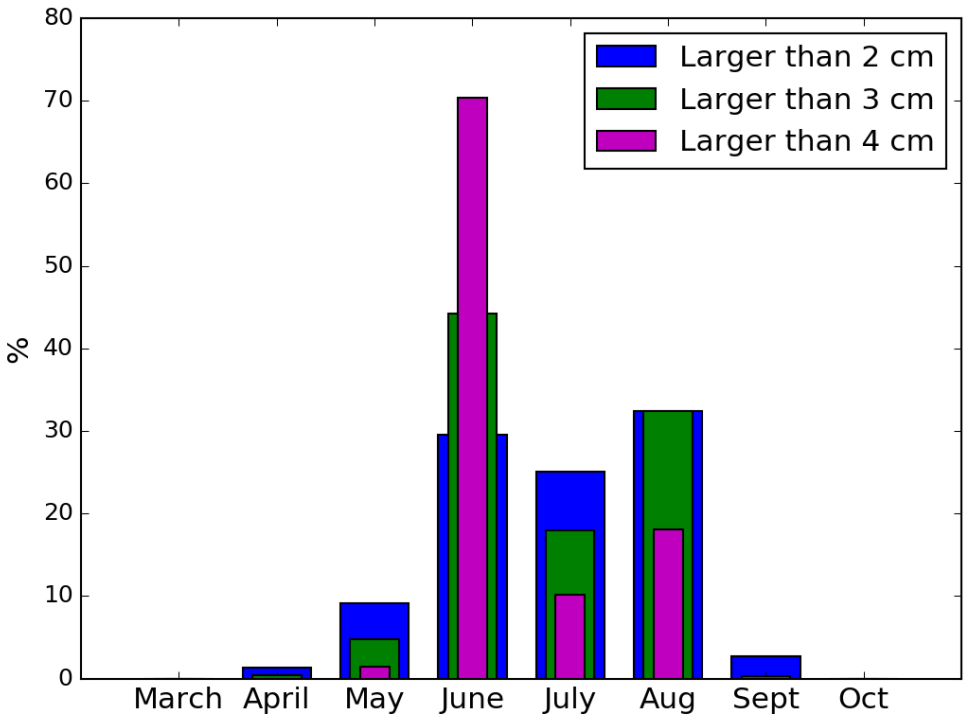


Figure 16: Frequency distribution for different hail classes per month in percent

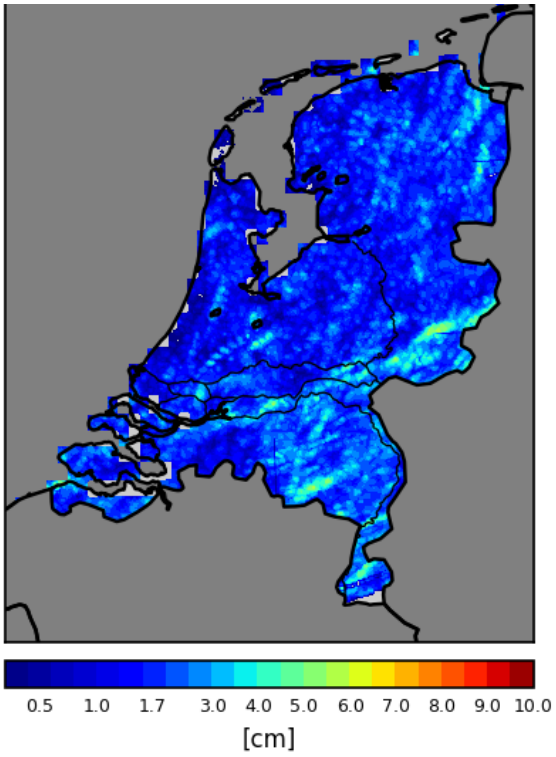


(a) Maximum Expected Hail Size (MEHS) between 2008 and 2016

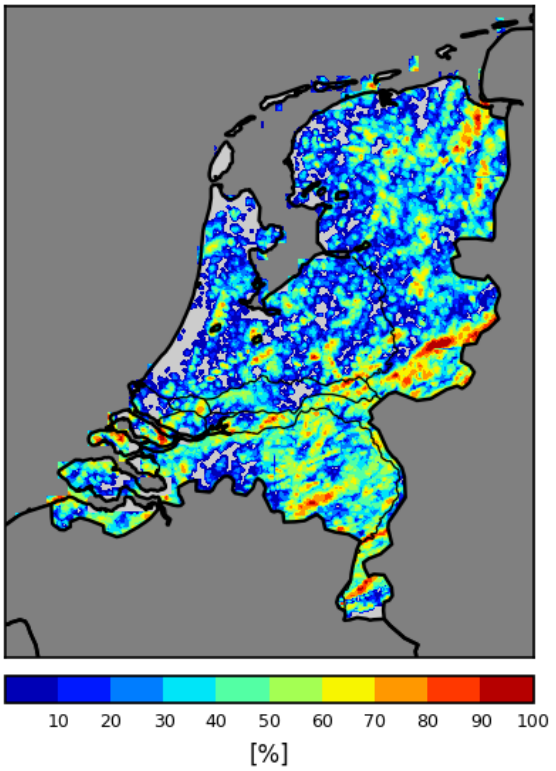


(b) The maximum Probability of Severe Hail (POSH) calculated between 2008 and 2016. For example, when the maximum POSH is 60%, it means that there is a 60% chance that severe hail (>2 cm in diameter) occurred at that location. The white areas indicate that probability was below 5% and thus is left empty.

Figure 17: Large hail climatology calculated by the algorithm developed by Witt et al. [1998]

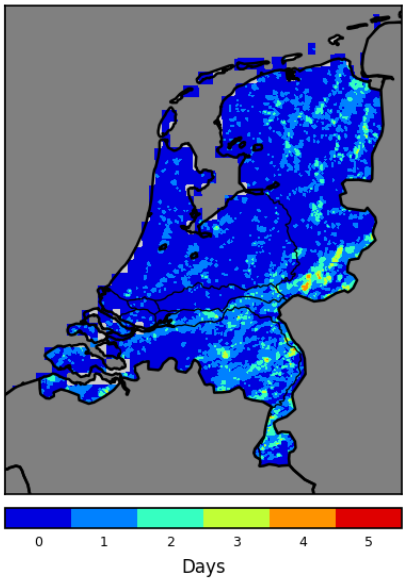


(a) Number of days where the MEHS is larger than 2 cm

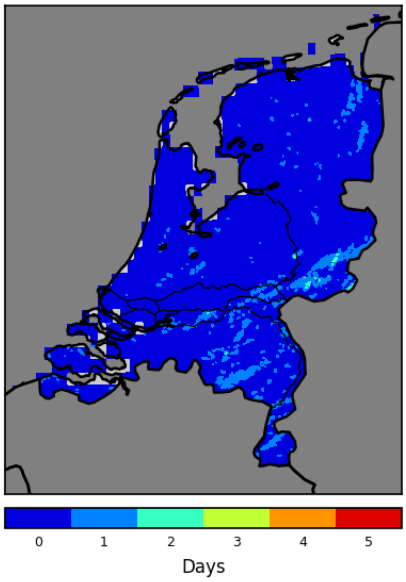


(b) Number of days where the MEHS is larger than 3 cm

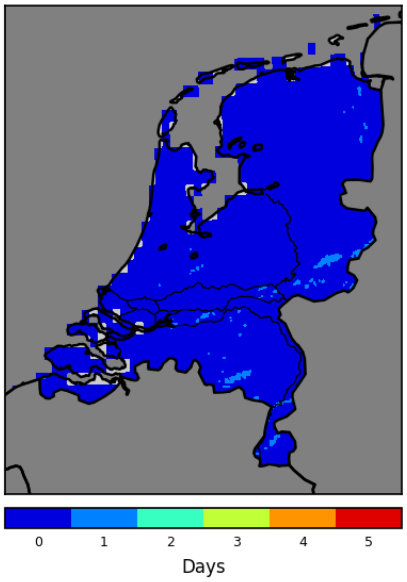


(c) Number of days where the MEHS is larger than 4 cm

Figure 18

# 7 Relation between meteorological parameters and hail size

In order to make a short-term prediction method for the occurrence of large hail, meteorological parameters, associated with large hail events, were investigated by consulting literature. Because most literature does not specifically focus on Europe (and more specifically, the Netherlands), it is important to use the conclusions made in literature and reproduce the analysis done in literature for the Netherlands.

## 7.1 Literature

### 7.1.1 Brooks [2009]

Research by Brooks [2009] focused on the product of CAPE[5] with SHR6 (vertical wind shear between 0 and 6 km above ground level), called the Energy Shear Index (ESI). It was found that the probability that soundings will be associated with significant severe thunderstorms (e.g. thunderstorms producing hail larger than 5 cm, wind gusts of at least 120kmh$^{-1}$ and/or an F2 tornado or more int) increases linearly with the ESI. For example, under conditions where the ESI is about 20000, the probability of a significant severe thunderstorm will be about 40% in Europe and 10% for the same ESI value in the United States. The difference between the two probabilities arises because there are more hills and mountains in areas where thunderstorms form in Europe than in the US. Since orography can be an important triggering mechanism, thunderstorms form more easily in Europe.

### 7.1.2 Brooks [2013]

Brooks [2013] investigated the occurrence of severe thunderstorms in the United States and Europe (European data provided by the ESWD). This was done by looking at over 1000 soundings made in these two continents and plotting the soundings in a WMAX-SHR6 space for both the US and Europe, where WMAX is defined as the maximum vertical velocity an air parcel can acquire according to the simple parcel theory[6]:

$$\text{WMAX} = \sqrt{2 * \text{CAPE}} \tag{27}$$

Including soundings associated with significant severe hail events and plotting this in the same WMAX-SHR6 space, a probability distribution can be made for significant severe hail (Figure 19a) by dividing the distribution of significant severe hail events by the unconditional probability of the sounding being observed. Interestingly, the probability of severe significant hail increases only with increasing deep layer (0-6 km) shear and appears not to be depending on the maximum vertical velocity. It appears that once the atmosphere is capable of producing a significant severe storm, the hail size does not change as a function of CAPE [Brooks, 2013]. In other words, when the conditions are favorable for significant severe thunderstorms, the probability of hail larger than 5cm is only a function of deep layer shear. Brooks [2013] also calculated the probability distribution for extremely large hail (hail larger than 7.5 cm) given a certain combination of WMAX and SHR6 (figure 19b), in which the probability for the occurrence of extremely large hail is also mostly depending on deep layer shear.

### 7.1.3 Púčik et al. [2015]

Another, more recent study by Púčik et al. [2015] investigated the sounding parameters associated with severe and non-severe thunderstorms in Europe only, using over 16000 proximity soundings for central Europe. In this study, the WMAX-SHR6 space was also used as a proxy for severe weather environments. They found that the probability for the occurrence of large hail, tornadoes, strong winds and heavy rain increases with higher values of WMAX and SHR6. Púčik et al. [2015] even found higher probabilities for the occurrence of large hail in high CAPE and high SHR6 soundings compared to the study done by Brooks [2013].

Púčik et al. [2015] also found an increase in average CAPE, deep layer shear, 800-600 hPa lapse rate, low level shear, mid-level shear for increasing storm severity. They conclude however, that (very) large hail typically occurs with high values of CAPE and that the probability increases when

[5] Brooks [2009] calculated CAPE using a mixed layer (ML) parcel
[6] Brooks [2013] calculated CAPE using a mixed layer (ML) parcel

conditions become more favorable for supercells (strong deep layer shear. LCL height and steep lapse rate between 800-600 hPa also increases for increasing hail size. Note that this study only investigated large hail being hail with diameters larger than 2 cm.

#### 7.1.4 Taszarek et al. [2017]

Taszarek et al. [2017] made a distinction between large hail and very large hail (2cm and 5cm, respectively). This research produces probability plots in the same way as done by Brooks [2013]. Taszarek et al. [2017] found that, given the situation a thunderstorm occurs, hail occurrence is greater with higher values for WMAX[7]. Other parameters used in research done by Taszarek et al. [2017] are 800-500 hPa temperature lapse rate, 0-500m above ground level mixed layer mixing ratio, and LCL height (Lifted condensation level). They finally conclude that the probability for large hail maximizes with high boundary layer moisture, steep mid- and low-level lapse rates and a high LCL height. When these thermodynamic conditions are available, the presence of hail larger than 5cm depends mainly on deep layer shear.

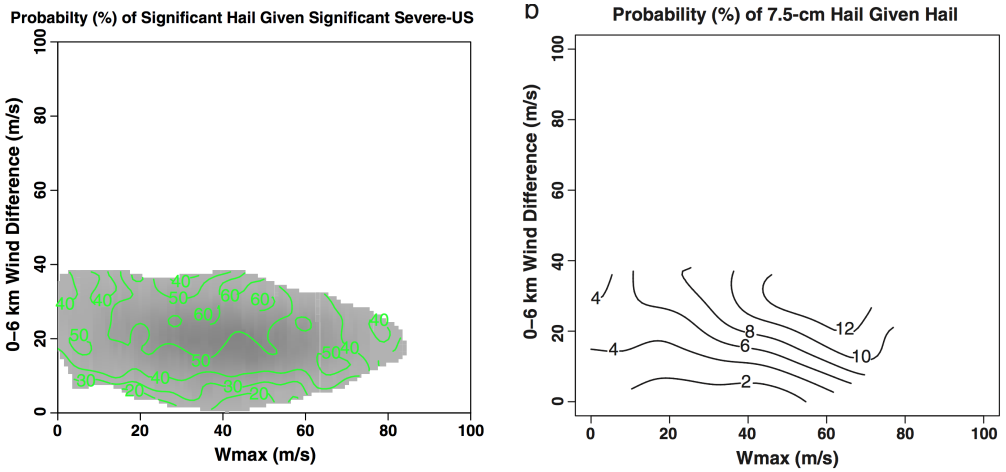


(a) (b)

Figure 19: Probability distribution of significant severe hail given the occurrence of a significant severe thunderstorm (Figure taken from Brooks [2013]) (left). Probability distribution of extremely large hail given the occurrence of significant severe hail (Figure taken from Brooks [2013]) (right).

Table 5: Overview of conclusions made by literature. '++' denotes that the paper is clear about the meteorological parameter is linked to to probability of hail or hail size. '+' denotes less important parameters discussed by the paper.

| Research | Large hail (>2cm) | Very large hail (>5cm) | Extremely large hail (>7.5cm) |
|---|---|---|---|
| Brooks [2013] | - | SHR6 (++) | SHR6 (++)<br>CAPE (++) |
| Púčik et al. [2015] | SHR6 (++)<br>CAPE (++)<br>LR86 (+)<br>LCL height (+) | - | - |
| Taszarek et al. [2017] | CAPE (++)<br>LCL height (+) | SHR6 (++)<br>CAPE (+)<br>LCL height (+) | -<br><br>- |

[7] Taszarek et al. [2017]. Given the situation that large hail occurs, the probability for very large hail (>5cm) is more dependent on SHR6 than on WMAX calculated CAPE using a mixed layer (ML) parcel through 0-500m above ground level

### 7.1.5 Johnson and Sugden [2014]

Johnson and Sugden [2014] investigated the relation of wind-related and thermodynamic parameters with hail size classes. They collected over 500 hail reports and used numerical weather prediction model data to obtain the vertical wind profile for each hail report. Eventually, the vertical wind profile for each hail size bin is averaged, resulting in composite hodographs for each hail size bin. The results are shown in figure 20. They found that the composite hodograph for hail sizes between 2 cm and 3 cm is different from hodographs belonging to larger hail size events. Especially the zonal wind vector being smallest of all classes. There is little difference in hodographs for hail sizes between 4 cm and 8 cm. When dealing with even larger hail (>8 cm), the average zonal wind is stronger and the average meridional wind weaker. Johnson and Sugden [2014] also introduced the Large Hail Parameter (LHP), of which the thermodynamic part is based on most unstable CAPE (MUCAPE), temperature lapse rate between 700 hPa and 500 hPa ($\mathrm{LR}_{7-5}$) and the hail growth zone thickness ($\mathrm{THK}_{\mathrm{HGZ}}$). MUCAPE is given by calculating the amount of CAPE for many air parcels starting at different heights in the lowest 30kPa layer of the atmosphere. The MUCAPE is then the one that gives the highest CAPE values [Stull, 2016]. The MUCAPE is then the CAPE at The wind related part is based on wind shear in the equilibrium level (0-1.5 km), the difference between the ground relative wind direction in the equilibrium level and the ground relative wind direction between 3-6 km ($\mathrm{GRW}_{\alpha\mathrm{EL}}$) and the difference between the storm relative wind direction between 3-6 km and the storm relative wind direction between 0-1 km ($SRW_{\alpha mid}$).

Johnson and Sugden [2014] uses statistical analyses to find that these parameters are best suited for this new parameter. This eventually leads to the Large Hail Parameter (LHP). The LHP consists of two parts: a thermodynamic part and a wind-related part:

$$\text{Thermodynamic} = \frac{\text{MUCAPE} - 2000}{1000} + \frac{3200 - \mathrm{THK}_{\mathrm{HGZ}}}{500} + \frac{\mathrm{LR}_{7-5} - 6.5}{2} \tag{28}$$

$$\text{Wind} = \frac{\mathrm{Shear}_{\mathrm{EL}} - 25}{5} + \frac{\mathrm{GRW}_{\alpha\mathrm{EL}} + 5}{20} + \frac{\mathrm{SRW}_{\alpha\mathrm{mid}} - 80}{10} \tag{29}$$

where the LHP is eventually defined as:

$$\text{LHP} = [\text{Thermodynamic} \times \text{Wind}] + 5 \tag{30}$$

Johnson and Sugden [2014] found that the parameter increases with increasing hail size.

### 7.1.6 Stull [2016]

Stull [2016] proposed a parameter for operational purposes which gives an indication whether or not large hail can occur. It uses meteorological parameters MUCAPE, shear between 0 and 6km, lapse rate between 700 hPa and 500 hPa and the temperature at 500 hPa. The Significant Hail Parameter (SHIP) is defined as follows:

$$\text{SHIP} = \frac{\text{MUCAPE} * \mathrm{LR}_{700-500\mathrm{hPa}} * \mathrm{Temperature}_{500\mathrm{hPa}} * \mathrm{Shear}_{0-6\mathrm{km}}}{4.2 * 10^7} \tag{31}$$

Where

$$\text{SHIP} = \begin{cases} \text{SHIP} * (\text{MUCAPE}/1300.) & \text{MUCAPE} < 1300 \\ \text{SHIP} * (\mathrm{LR}_{700-500\mathrm{hPa}}/5.8) & \mathrm{LR}_{700-500\mathrm{hPa}} < 5.8 \end{cases} \tag{32}$$

The SHIP ranges between 0-4. It is been assumed that if the SHIP>1, pre-storm conditions are favorable for very large (significant) hail (hail larger than 5cm in diameter). Stull [2016] notes that if the SHIP is larger than 1.5, significant hail is frequently observed.

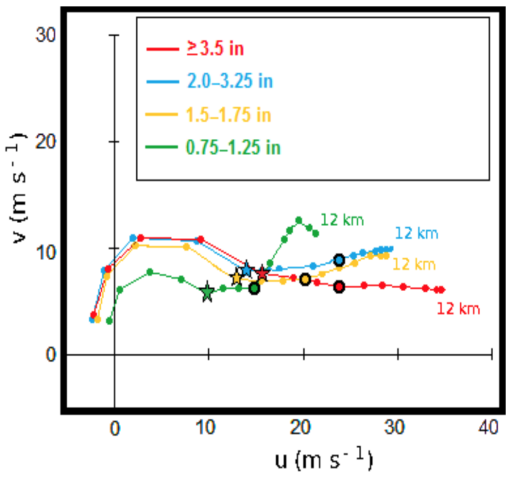


Figure 20: Composite hodographs for different hail size classes for the United States. Figure was taken from Johnson and Sugden [2014]

## 7.2 Analysis for the Netherlands

In order to reproduce the analyses done by literature described in the previous section, the MEHS calculated with the HDA by Witt et al. [1998] is used as an observation. Using the HDA as a proxy results in very high resolution measurements of large hail events. Since the chances of errors in the HDA increases with distance from the radar, only HDA calculations within the borders of the Netherlands are used. An overview of the reproduced parameters in this thesis is shown in table 6.

For every selected day (where CAPE>1500 J/kg and CIN>-100 J/kg) between 2010 and 2016, the HIRLAM runs shown in table 2 are used. Due to the large temporal variability in hail size, a time window is used in which the maximum hail size is determined. This time window is set to ± 2 hour with respect to the HIRLAM run time.

In order to form severe thunderstorms in the first place, large amounts of CAPE must be present. It is chosen that all other parameters are retrieved from the location with the highest CAPE value. Next, the HDA determines the maximum hail size present in the whole domain for each time window. This maximum hail size is compared with the parameters retrieved from the location with the highest CAPE value (figure 22). A second analysis is done in which the maximum hail size is determined for every day. This hail size is then compared with the outcome of every HiRLAM run (figure 23). A third analysis compares the maximum value of each parameter per day with the maximum hail size per day (figure 34). Finally, the fourth analysis compares CAPE values under low shear (pulse storm) and high shear (supercell) situations with hail size per time window (as in the first analysis) shown in figure 25.

Table 6: Parameters used

| Parameter | Level | Unit |
|---|---|---|
| CAPE | Most unstable | J $kg^{-1}$ |
| Shear | 0-6km | $ms^{-1}$ |
| Lapse rate | 800-600 hPa | K $m^{-1}$ |
| LCL | - | m |
| ESI | - | $m^3s^{-3}$ |
| Specific humidity | Surface | g $kg^{-1}$ |
| Mixing ratio | - | kg $kg^{-1}$ |
| SHIP | - | - |
| LHP | - | - |

### 7.2.1 CAPE and shear

The results of the analysis shown in figure 22a show that there is indeed an increase in average MUCAPE with increasing hail size. The main feature which can be seen in this analysis is that in situations where hail sizes were calculated smaller than 2 cm, the amount of MUCAPE at that moment is significantly smaller than during large hail events (>2 cm). This feature is also visible in the second analysis (figure 23a), using the maximum hail size per day. Even though there is more spread in the MUCAPE values, the hail size bins are more evenly filled and thus the results are more reliable for larger hail sizes. The third analysis shows (figure 24a an increase in average MUCAPE with hail size. However, these hail size bins are much smaller and thus resulting in less reliable outcomes.

Looking to the amount of shear between 0 and 6 km (Figure 22b), no clear trend is visible. According to Brooks [2013], the hail size is only increasing with shear during events producing >5 cm hail. Because of the small number of occurrences, this is not visible in the first analysis. The second and third analysis (figure 23b and 24b) show the same features.

Figure 25 shows the CAPE values compared with hail sizes under low and high shear conditions, indicating conditions favorable for pulse- and supercell storms, respectively. Pulse storms are vertically towering thunderstorms which form in conditions lacking strong vertical wind shear. These storms have their updraft in the same location as their downdraft, eventually cutting of the inflow of air into the storm shortly after the storm formed. Because of the short lifetime, pulse storms often do not produce very large hail. Since hail grows the longer the hail can be supported by the updraft, theoretically the vertical wind speed is related to the maximum hail size which can be supported by the updraft. When the terminal velocity of a hailstone is reached, the hail will fall to the ground. So the higher the vertical velocity (e.g. CAPE), the larger the hail stone can possibly grow. In supercell storms shear causes the storm to tilt and this relation with CAPE does not hold, even though supercell storms can support very large hail.

### 7.2.2 LCL, Specific humidity, lapse rate and ESI

Looking at the temperature lapse rate between 700hPa and 500hPa (figure 22c, 23c and 24c), no clear relation is visible with the hail size. Also, the LCL height shows little correlation for all analyses (figure 22d, 23d and 24d). Specific humidity seems to have a higher value with increasing hail size in all analyses. However, since the MUCAPE is depending on humidity, it is possible that some intercorrelation exists between MUCAPE and specific humidity. The Energy Shear Index shows a higher average value with hail sizes larger than 4cm in all analyses. However, the amount of observations in these hail size bins is very small.

### 7.2.3 Large Hail Parameter

Because the amount of shear has to be at least 14 m/s in order to calculate the LHP, only a fraction of the observations remain. For the remaining points, there is no clear trend between the Large Hail Parameter and the hail size (figure 22g). In the second and third analysis (figure 23g and 24g), no clear improvement is visible.

### 7.2.4 Significant hail parameter

Even though the significant hail parameter is developed to indicate the chance of significant hail (>5 cm) which only occurred two times in this dataset, a relation with the hail size seems visible (figure 22h), even in smaller hail size classes. The two significant hail observations both have values larger than 1.0, at which according to Stull [2016] the minimum value for conditions favorable for significant hail. In the second and third analysis (figure 23h and 24h), there is a small increase in SHIP with increasing hail size. The largest hail size class have average values above 1.0.

### 7.2.5 Hodograph composite

The resulting hodograph composites are shown in figure 21. At first sight, we see a large difference between the composite hodograph of Johnson and Sugden [2014], as in their research the zonal wind vector is much higher with respect to the composite hodograph produced in this thesis. The meridional wind vector however, is about the same magnitude. The results show that there is some distinction between the different hail size classes. It seems that the class with hail sizes

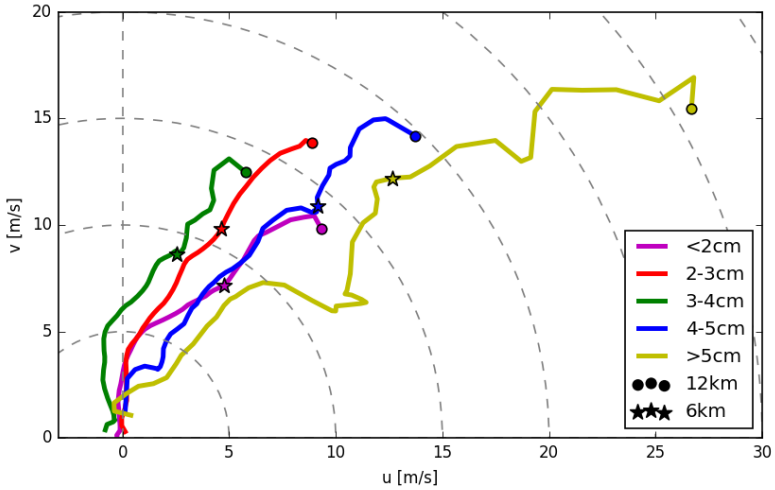


Figure 21: Composite hodograph for the hail events between 2010 and 2016 for different hail size classes.

smaller than 2cm have an average hodograph in which the zonal wind vector is about the same magnitude as the meridional wind vector. The shape of this hodograph does not differ much from the hodographs of larger hail classes (2-3cm and 3-4cm). However, when looking at the largest two hail classes, there seems to be an increase in zonal wind velocity with height. Especially with hail sizes larger than 5cm. Unfortunately, the amount of very large hail events in the Netherlands is much smaller than in the United States. Therefore, this composite hodograph is less reliable than the one made by Johnson and Sugden [2014].

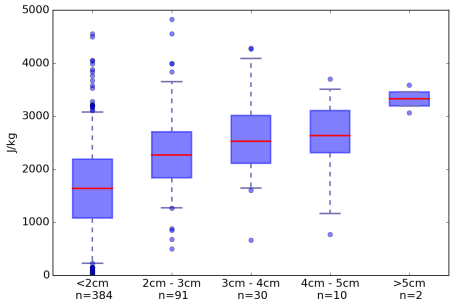


(a) MUCAPE

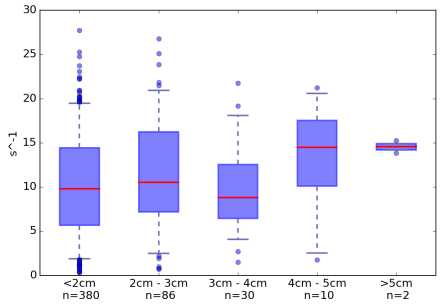


(b) Shear between 0-6km

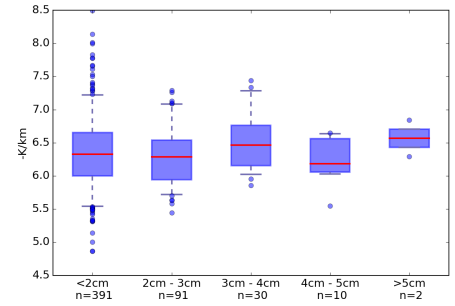


(c) 700-500hPa lapse rate

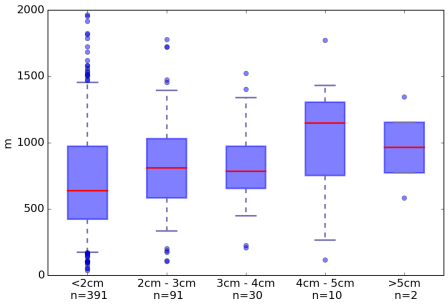


(d) Lifted Condensation Level

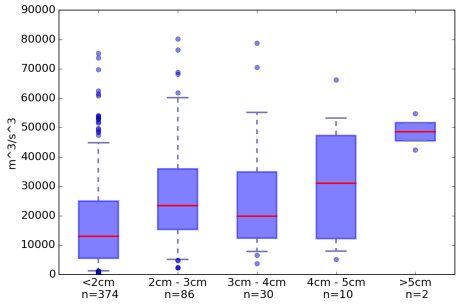


(e) Energy Shear Index (ESI)

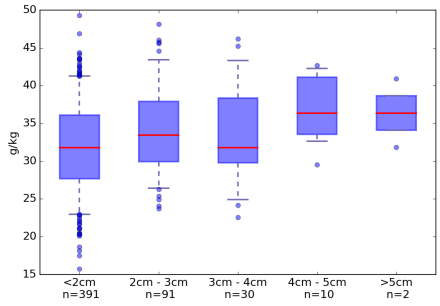


(f) Specific humidity

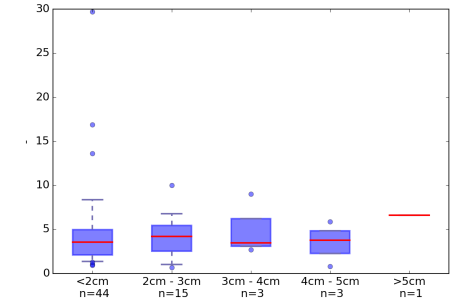


(g) Large hail parameter

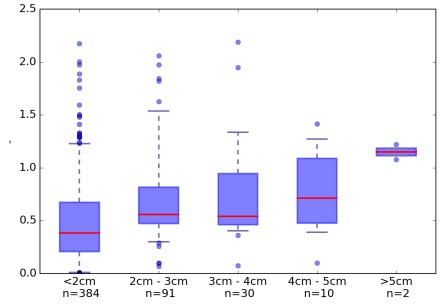


(h) Significant hail parameter

Figure 22: Boxplots for several meteorological parameters compared with hail size bins shown on the x-axis using a time window of ±2 hours. The size of each hail size bin is shown below the x-axis. The red line shows the median, the blue box denotes the 25th and 75th percentiles and the whiskers show the 5th and 95th percentiles.

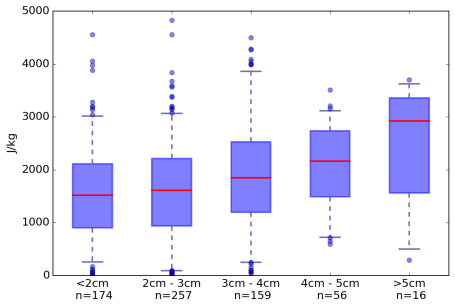


(a) MUCAPE

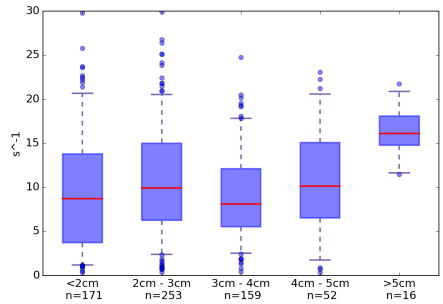


(b) Shear between 0-6km

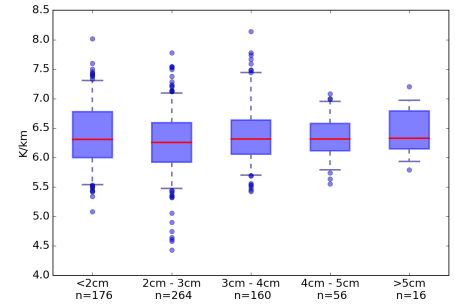


(c) 700-500hPa lapse rate

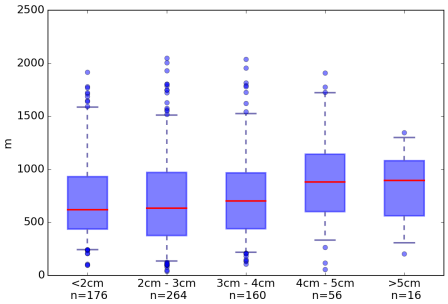


(d) Lifted Condensation Level

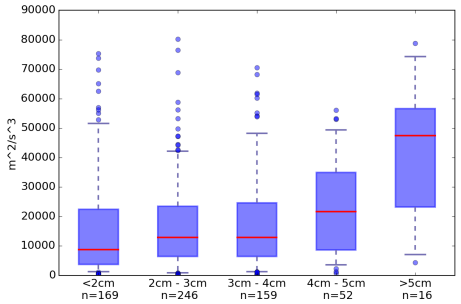


(e) Energy Shear Index (ESI)

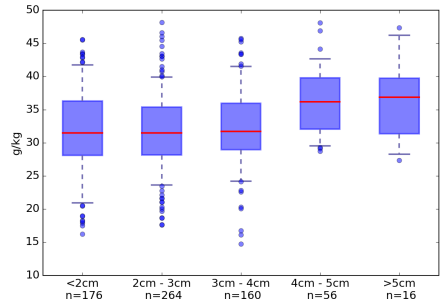


(f) Specific humidity

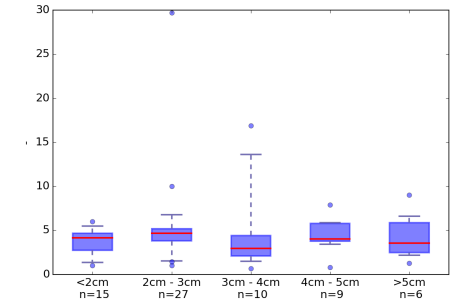


(g) Large hail parameter

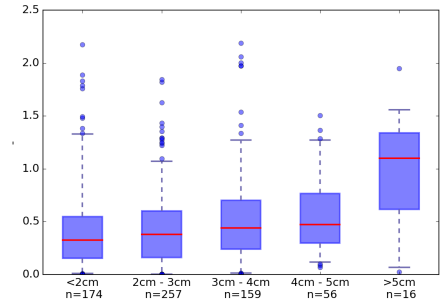


(h) Significant hail parameter

Figure 23: As in figure 22, but each parameter is now compared with the maximum hail size calculated per day

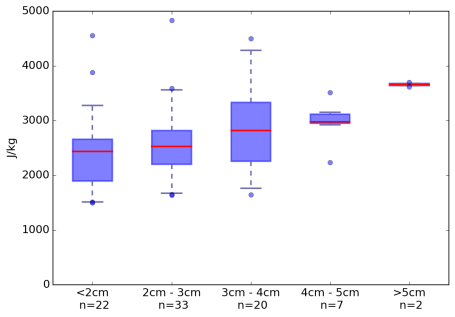


(a) MUCAPE

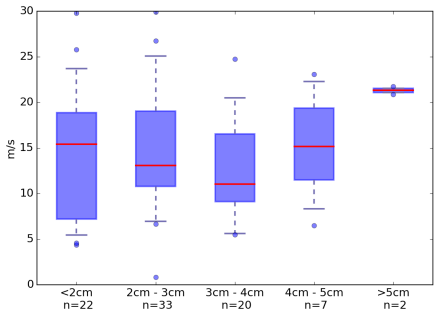


(b) Shear between 0-6km

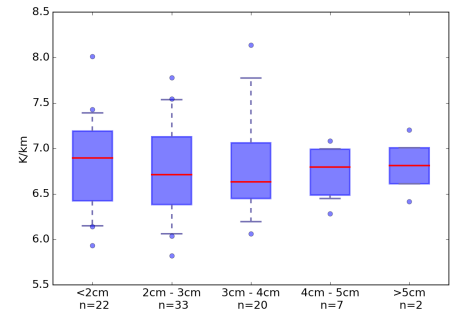


(c) 700-500hPa lapse rate

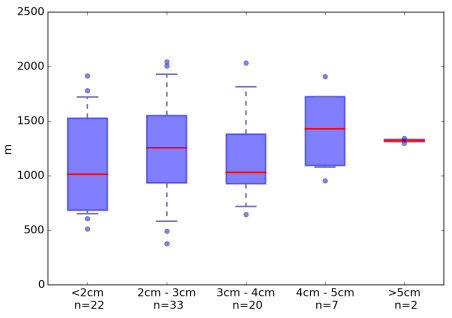


(d) Lifted Condensation Level

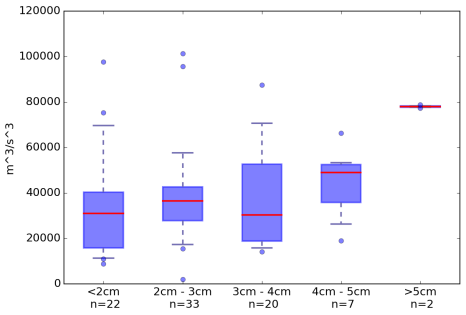


(e) Energy Shear Index (ESI)

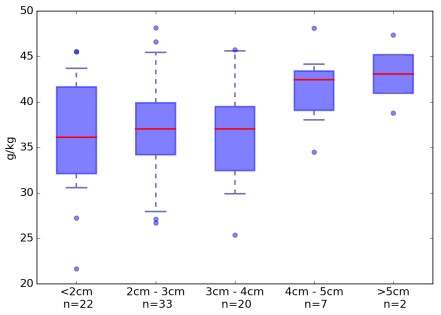


(f) Specific humidity

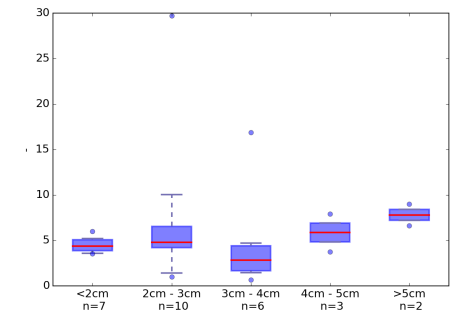


(g) Large hail parameter

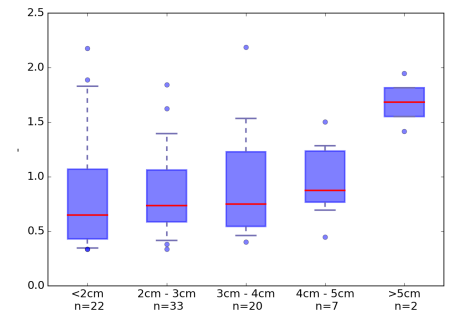


(h) Significant hail parameter

Figure 24: As in figure 22, but each parameter is now compared with the maximum hail size calculated per day

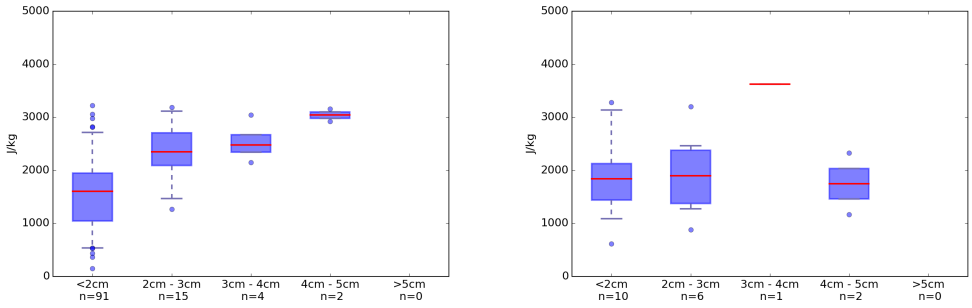


(a) Deep layer shear $< 5.144$ m/s

(b) Deep layer shear $> 20.577$ m/s

Figure 25: As in figure 22, but each now for MUCAPE under low and high shear conditions

## 7.3 Conclusions/summary

Multiple analyses are done to find meteorological parameters which are related to hail size. Analyses of the parameters LR75, LCL and LHP show that there is no significant increase in parameter value with increasing hail size. CAPE, shear, ESI and SHIP do show an increase above hail sizes of about 4 to 5 cm. Brooks [2013] states that once the atmosphere is capable of producing significant severe thunderstorms, the hail size only changes as a function of shear. Unfortunately, this conclusion cannot be reproduced since in the Netherlands, events producing hail sizes larger than 5 cm are very rare. Taszarek et al. [2017] concluded that given the situation a thunderstorm occurs, hail occurrence is greater with increasing values of WMAX. Even though this study concludes that the probability of large hail increases with increasing WMAX, the analyses done in this thesis show a same result in the average hail size with increasing CAPE (related to WMAX, equation 27): the average CAPE increases with hail size, at least until hail sizes of about 5 cm. The weak trend in deep layer shear is in line with the conclusions reached by Brooks [2013] and Taszarek et al. [2017]. When the CAPE is weak, the hail size does not increase with increasing shear, simply because thunderstorms are not triggered with small amounts of CAPE. However, very large hail events (>5cm) all occur in situations where the shear is higher than average. The ESI is developed to highlight situations where the amount of CAPE and shear are both high. Especially in the second analysis, the ESI indeed shows much higher values during very large hail events. Therefore, the ESI can be useful in highlighting areas where conditions are favorable for very large hail. Also the significant hail parameter is developed to determine whether or not a certain sounding can produce large hail. The results are similar to those of ESI, probably because of the dependence of SHIP on MUCAPE and deep layer shear.

It is clear the most of the parameters do not show a clear relation with hail sizes smaller than 4 to 5cm. Only the MUCAPE increases steadily from hail sizes smaller than 2 cm to hail sizes larger than 5 cm. Especially the minimum amount of MUCAPE needed for a certain hail increases with MUCAPE under low wind shear conditions. Therefore only MUCAPE can be of value when predicting hail sizes between 2 and 5 cm. ESI and SHIP can be used as an addition to forecast hail sizes larger than 5 cm.

# 8 Hail size prediction and forecast product

Because large hail can cause severe damage to property and people, it is of great importance that meteorologists can issue warnings for (very) large hail in a specific area. Based on the analyses done and conclusions made in the previous section, an attempt has been done to create a hail size forecast and hail probability product. Next, skill score analyses are done to test the reliability of the products. Finally, the products are used on some case studies.

## 8.1 Hail size forecast product

The goal of the hail size prediction product is to give an estimation of the maximum hail size which can occur in a certain atmospheric condition. Based on the conclusions made in the previous section, a relation can be found between MUCAPE and the maximum hail size. The previous section concluded that hail sizes up to 5 cm in diameter are related with MUCAPE under conditions with small amounts of wind shear. To assess the relation of hail size with MUCAPE under different shear conditions, three shear classes are made: <5.144 m/s (very low), 5.144 - 10 m/s (low) and 10 - 15 m/s (medium). Scatter plots of these three classes vs. hail size are shown in figure 26. To

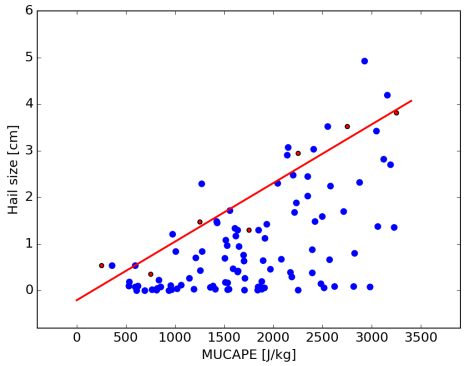


(a) Scatter plot of MUCAPE vs. hail size under shear conditions of less than 5.144 m/s

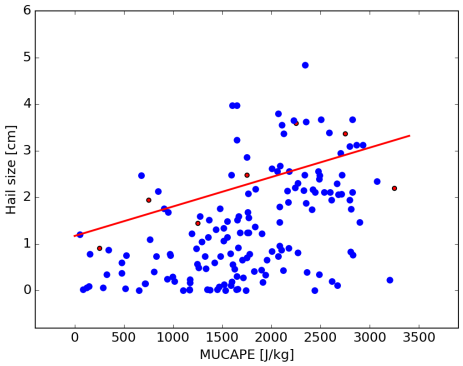


(b) Scatter plot of MUCAPE vs. hail size under shear conditions between 5.144 and 10 m/s

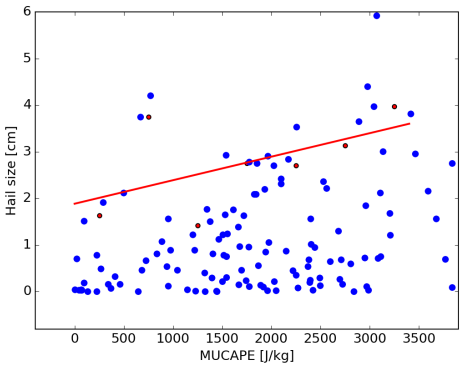


(c) Scatter plot of MUCAPE vs. hail size under shear conditions between 10 and 15 m/s

Figure 26

create a linear relation of the maximum hail size possible under certain MUCAPE values, seven MUCAPE classes are made (0-500 J/kg, 500-1000 J/kg, 1000-1500 J/kg, 1500-2000 J/kg, 2000-2500 J/kg, 2500-3000 J/kg and 3000-3500 J/kg). For each of these classes, the 90th percentile of hail size is calculated. This results in 7 points over which a polynomial fit has been applied (red line in the scatter plots). The resulting polynomial fits give estimates of the maximum hail size (MHS) possible given the amount of MUCAPE for the different shear classes:

$$\mathrm{MHS_{VL}} = 0.001258 \cdot \mathrm{MUCAPE} - 0.207586 \tag{33}$$

$$\mathrm{MHS_L} = 0.000632 \cdot \mathrm{MUCAPE} + 1.171771 \tag{34}$$

$$\mathrm{MHS_M} = 0.000505 \cdot \mathrm{MUCAPE} + 1.884879 \tag{35}$$

The indices VL, L and M indicate the different shear classes (very low, low and medium). Remarkably, the upper boundary in hail size is only well visible in during conditions with very low deep layer shear. Low shear and medium shear do not show the upper boundary in hail size very well. The polynomial fits also show very small slopes and therefore are not very useful in hail size forecasting products. Theoretically, this can be explained by the fact that during very low shear conditions, the storm is almost vertical and hailstones only travel in the vertical direction and not in the horizontal direction. The maximum possible hail size is then achieved when the terminal velocity of the hail stone is equal to the updraft velocity. The terminal velocity of a falling sphere is defined by Khvorostyanov and Curry [2005] as

$$V_t = \left( \frac{2 g v_b}{C_D A} \left| \frac{\rho_b}{\rho_F} - 1 \right| \right)^{1/2} \tag{36}$$

where $v_b$ is the volume of the spherical body, $A$ is the projected area, fluid density $\rho_F$ through which the body is moving, body density $\rho_b$ and the drag coefficient $C_D$. Using the fact that

$$v_b = \frac{4}{3} \pi r^3 \tag{37}$$

and

$$A = 4 \pi r^2, \tag{38}$$

equation 39 can be rewritten as

$$V_t = \left( \frac{g \frac{4}{3} D}{C_D} \left| \frac{\rho_b}{\rho_F} - 1 \right| \right)^{1/2} \tag{39}$$

Recalling the maximum vertical velocity which can be achieved by a given value of MUCAPE:

$$V_{\max} = \sqrt{2 * \mathrm{MUCAPE}} \tag{40}$$

Since the maximum hail size is achieved when $V_t = V_{\max}$, the following equation holds

$$\left( \frac{g \frac{4}{3} D}{C_D} \left| \frac{\rho_b}{\rho_F} - 1 \right| \right)^{1/2} = \sqrt{2 * \mathrm{MUCAPE}} \tag{41}$$

Rewriting equation 41 results in a relation between MUCAPE and maximum hail stone diameter:

$$D_{\max} = \mathrm{MUCAPE} \left( 2 \frac{C_D \rho_F}{\frac{4}{3} g \rho_b C_H} \right) \tag{42}$$

Assuming $\rho_F = 0.6 \mathrm{kg/m^3}$, $\rho_b = 920 \mathrm{kg/m^3}$ and a corresponding drag coefficient of $C_D \approx 1$, which is about the same order as found by Khvorostyanov and Curry [2005], the maximum hail size is about a factor 10 too large. Physically, this overestimation is probably due to the limited amount of time available for the hail stone to develop since pulse storms are relatively short lived (less than an hour). To correct for this, a 'hail coefficient' $C_H$ is introduced. Also, note that the drag coefficient depends strongly on shape. Since the shape of hail stones can vary a lot, the drag coefficient can change drastically (factor 2 maximum). Equation 42 illustrates that the linear fit through the observations has a legitimate physical meaning. The assumption that the updraft velocity equals the terminal velocity of the hail stone when reaching maximum hail size is only applicable at very low shear conditions. When shear increases, the hailstones do not travel only in the vertical, but can travel horizontally and therefore this relation does not hold. In appendix C equation 33 is applied to the HIRLAM MUCAPE field during very low shear conditions. To assess the forecast skill of this hail size prediction product, it is necessary to compare the outcomes with an independent dataset of hail sizes. Since this is not available at the moment, it is not possible to do a forecast skill analysis.

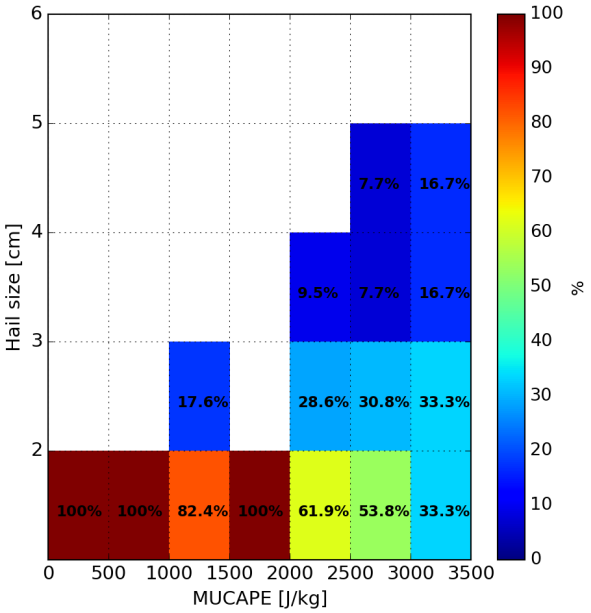


Figure 27: Probability distribution for very low shear situations indicating the probability a certain hail size will occur during certain MUCAPE conditions based on historical data

## 8.2 Probability product

Next, a hail size probability distribution is made based on historical data (e.g. on analyses done in the previous section). This product has binned both the hail size and MUCAPE, such that given a value of MUCAPE, the probability for the occurrence of a certain hail size based on historical data is shown. This is only done for very low shear situations, since these situations allow for the undisturbed dependence of MUCAPE on hail size according to equation 42. The resulting probability distribution is shown in figure 27. One can use this probability distribution to assess the probability for the occurrence of a certain hail size class given the amount of MUCAPE. For example, under conditions where the MUCAPE is between 2000 and 2500 J/kg, there is a 28.6% chance that hail sizes occur between 2 and 3cm based on historical data. Note that the timespan of the data is insufficient to give a climatological percentage. So it is important to note that the probability is based on data between 2008 and 2016.

# 9 Conclusions/Recommendations

It has been shown that is is possible to apply a HDA on the Dutch radars in combination with HIRLAM temperature data. Some difficulties can arise due to ground clutter, but they are eventually filtered out with success. It is important to note that the HDA made by Witt et al. [1998] is not designed to give actual hail size, but gives an indication of what is possible a specific storm. To increase the reliability of the HDA, it must be improved by, for example, using dual-polarization radars. These radars can give important information about the precipitation type and therefore can be used in improving the HDA made by Witt et al. [1998]. Nevertheless, a climatology of large hail was successfully made. The 9-year climatology indicates that large hail is most likely in the (south) east of the Netherlands. However, to conclude about large hail climate in the Netherlands, a dataset of at least 30-years has to be available. Finally, it was investigated what meteorological parameters are associated with large hail events. Outcomes of the analyses show that MUCAPE was the only parameter which shows correlation with hail size, especially when deep layer shear is weak. In the Netherlands, not many situations occurred in which strong wind shear is combined with large amounts of MUCAPE. Therefore, the main focus on developing a hail size prediction product was during very low shear conditions (deep layer shear below 5.144 m/s). It was found that there was an upper boundary in hail size with increasing MUCAPE. Combining the upper boundary with a physical theory, a Maximum Hail Size (MHS) product was created which gives an indication of the maximum possible hail size under certain MUCAPE conditions when very weak shear is present. To assess the probability of a certain hail size to occur under very low shear conditions, a probability product was made based on historical data. Both products can eventually be used in operational meteorology. However, to have an indication of hail size or probability of a certain hail size under somewhat stronger shear conditions, more observations are needed in order to find a stronger relationship between meteorological parameters and hail size. To assess the prediction skill for both products, it is necessary to compare the product with an independent observed hail size dataset.


# Acknowledgements

I would like to thank my Dr. Aarnout van Delden (IMAU) and Dr. Sander Tijm (KNMI) for the great supervision of this research. Also, a special thanks to Rob Sluijter (KNMI) in creating many possibilities to improve my presentation skills and introducing my work to insurers. Also, thanks to the ESSL (European Severe Storms Laboratory) for providing me with hail (size) observation data.

# A Clutter filter

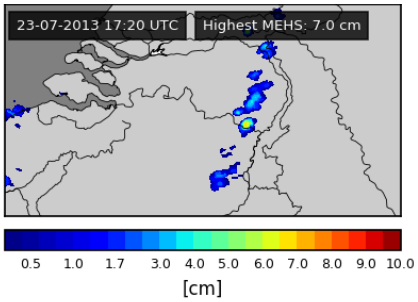


(a) Without filter

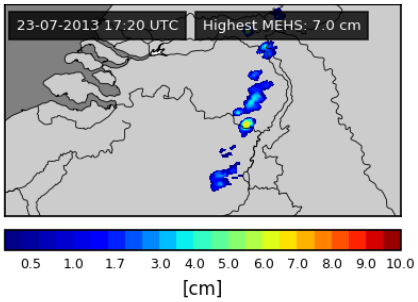


(b) With filter

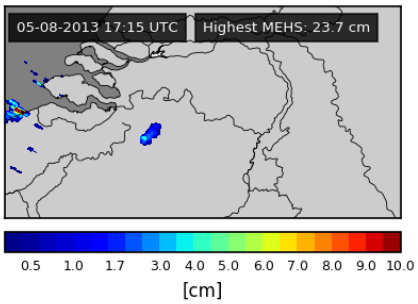


(c) Without filter

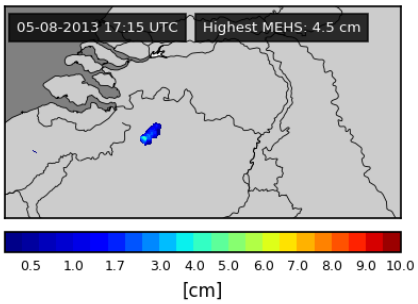


(d) With filter

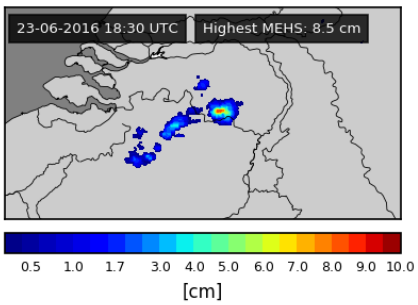


(e) Without filter

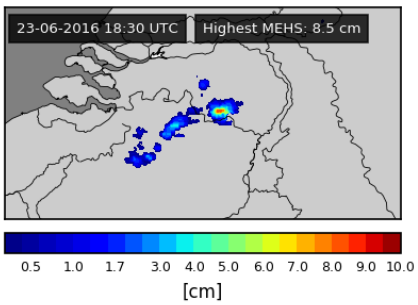


(f) With filter

Figure 28: Overview of the MEHS for different cases which are used to test the filtering technique. Note that the absolute values of the HDA are incorrect as they are used in a test phase of the HDA.

Table 7: Maximum hail size present in domain

| Date and time | Without filter | With filter | Clutter present | Clutter removed |
|---|---|---|---|---|
| 23-07-2013 17:15 | 7 cm | 7 cm | Yes | Yes |
| 05-08-2013 17:20 | 23.7 cm | 4.5 cm | Yes | Yes |
| 23-06-2016 18:30 | 8.5 cm | 8.5 cm | No | No |

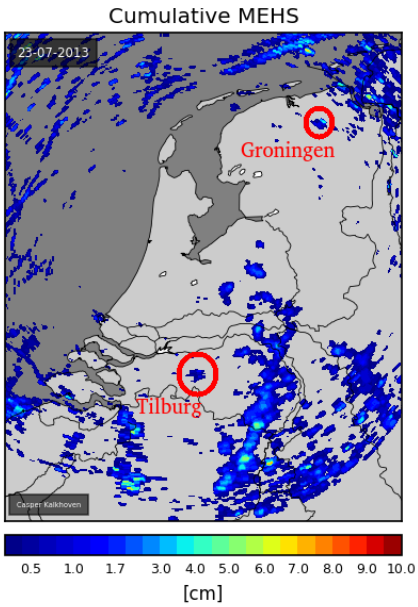


(a) Cumulative MEHS for 23-7-2013. Lots of ground clutter is visible. Also the cities Tilburg and Groningen are visible as ground clutter.

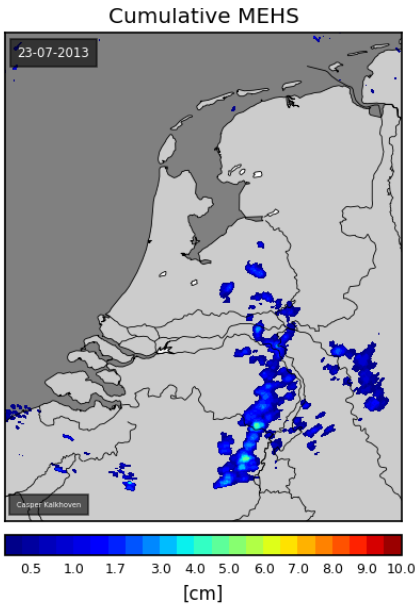


(b) Cumulative MEHS for 23-7-2013 after applying the ground clutter filter and ignoring the lowest scan.

Figure 29

# B Correcting for tilt

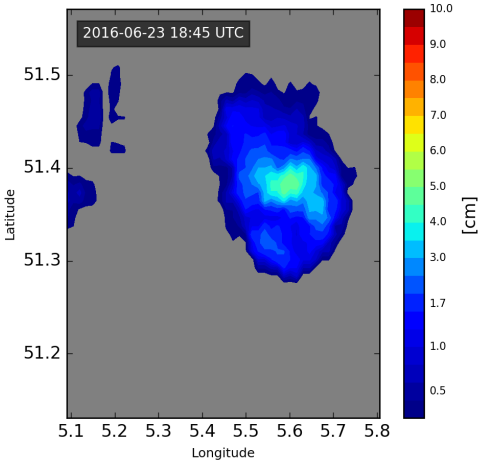


(a) Original HDA output (MEHS without filtering for storm tilt)

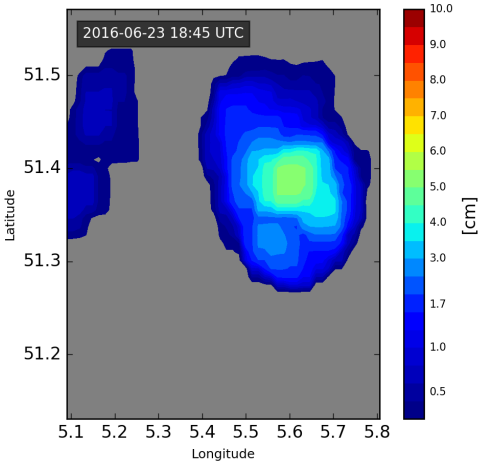


(b) MEHS with morphological dilation applied

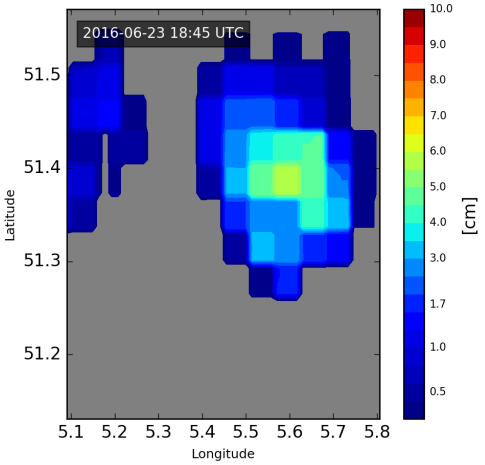


(c) MEHS applied on 4x4km grid

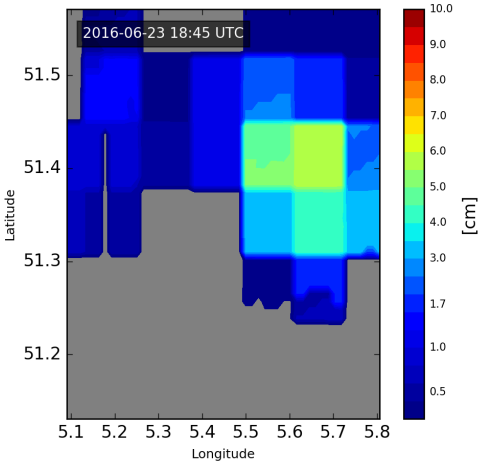


(d) MEHS applied on 8x8km grid

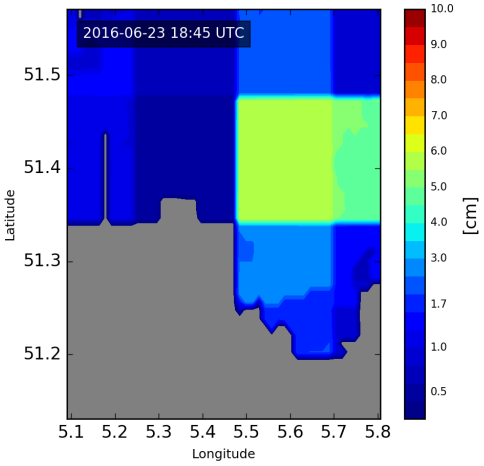


(e) MEHS applied on 15x15km grid

# C Forecasting tool

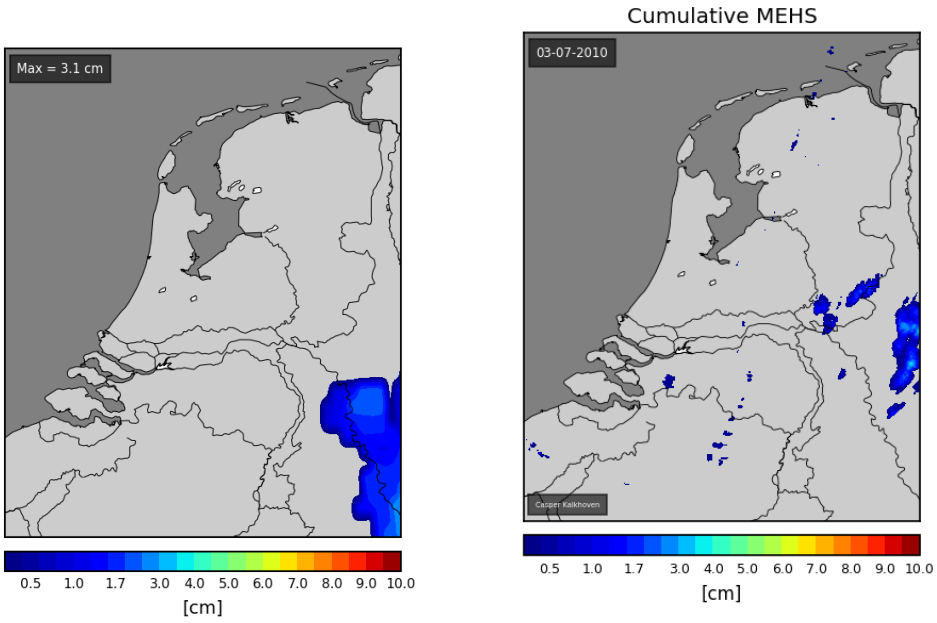


Figure 31: Applying equation 33 to the MUCAPE field of HiRLAM during very low shear conditions (left) and the cumulative calculated hail size by using the HDA (right) at 03-07-2010

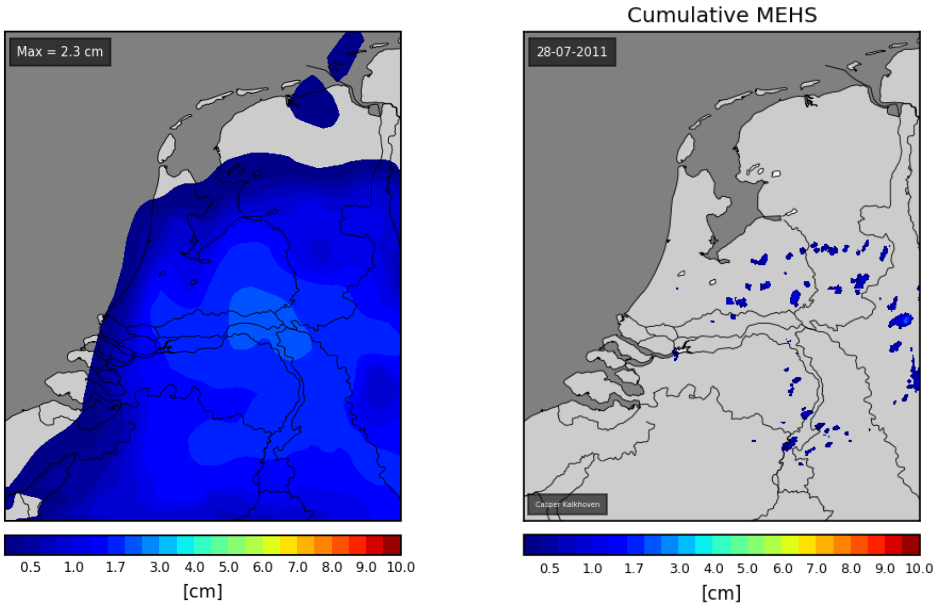


Figure 32: Applying equation 33 to the MUCAPE field of HiRLAM during very low shear conditions (left) and the cumulative calculated hail size by using the HDA (right) at 28-07-2011

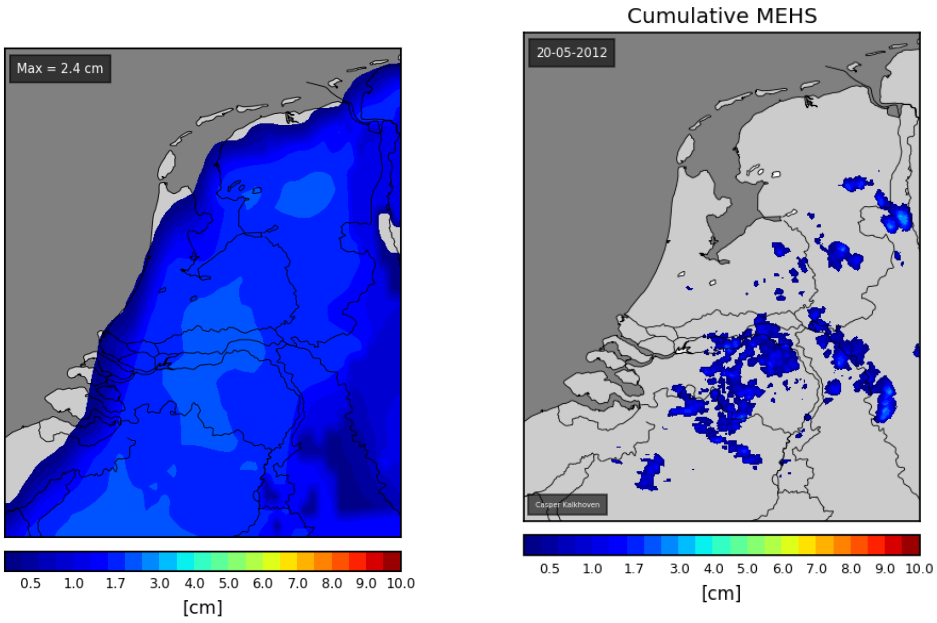


Figure 33: Applying equation 33 to the maximum MUCAPE field of HiRLAM during very low shear conditions (left) and the cumulative calculated hail size by using the HDA (right) at 20-05-2012

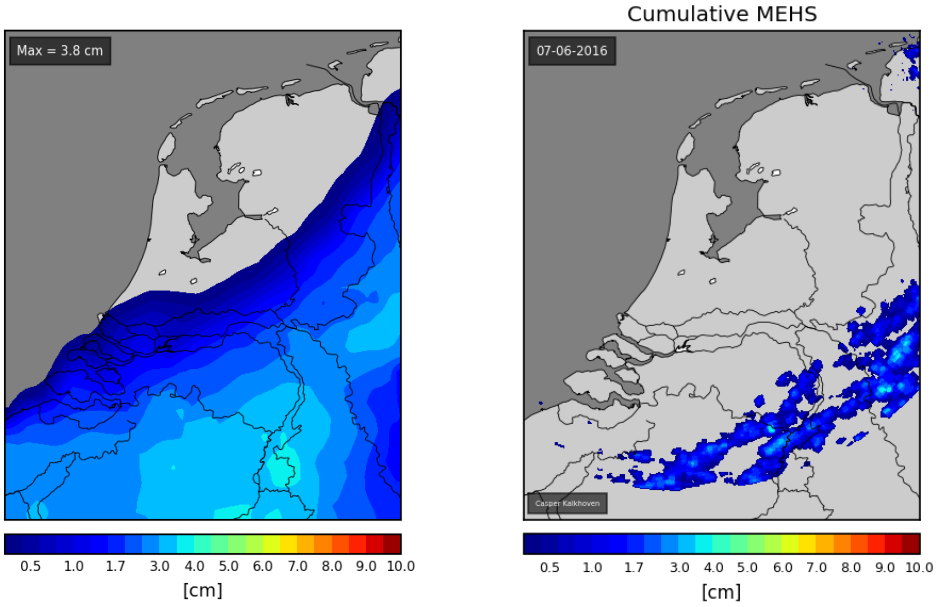


Figure 34: Applying equation 33 to the maximum MUCAPE field of HiRLAM during very low shear conditions (left) and the cumulative calculated hail size by using the HDA (right) at 07-06-2016

# References


Steven a. Amburn and Peter L. Wolf. VIL Density as a Hail Indicator. *Weather and Forecasting*, 12(3):473–478, 1997. ISSN 0882-8156. doi: 10.1175/1520-0434(1997)012<0473:VDAAHI>2.0.CO;2.

August H. Auer Jr. Hail Recognition Through the Combined Use of Radar Reflectivity and Cloud-Top Temperature, 1994. ISSN 00270644.

L.J. Battan. Radar observation of the atmosphere. L. J. Battan (The University of Chicago Press) 1973. PP X, 324; 125 figures, 21 tables. £7·15. *Quarterly Journal of the Royal Meteorological Society*, 99(422):793–793, 10 1973. ISSN 00359009. doi: 10.1002/qj.49709942229. URL http://doi.wiley.com/10.1002/qj.49709942229.

Hans Beekhuis and Iwan Holleman. From Pulse to Product , Highlights of the digital-if upgrade of the Dutch national radar network. pages 1–3, 2010.

H. E. Brooks. Severe thunderstorms and climate change. *Atmospheric Research*, 123:129–138, 2013. ISSN 01698095. doi: 10.1016/j.atmosres.2012.04.002. URL http://dx.doi.org/10.1016/j.atmosres.2012.04.002.

Harold E. Brooks. Proximity soundings for severe convection for Europe and the United States from reanalysis data. *Atmospheric Research*, 93(1-3):546–553, 2009. ISSN 01698095. doi: 10.1016/j.atmosres.2008.10.005. URL http://dx.doi.org/10.1016/j.atmosres.2008.10.005.

John L. Cintineo, Travis M. Smith, Valliappa Lakshmanan, Harold E. Brooks, and Kiel L. Ortega. An Objective High-Resolution Hail Climatology of the Contiguous United States. *Weather and Forecasting*, 27(5):1235–1248, 2012. ISSN 0882-8156. doi: 10.1175/WAF-D-11-00151.1. URL http://journals.ametsoc.org/doi/abs/10.1175/WAF-D-11-00151.1.

B. Federer and A. Waldvogel. Hail and Raindrop Size Distributions from a Swiss Multicell Storm, 1975. ISSN 0021-8952.

Douglas R Greene and Robert A. Clark. Vertically Integrated Liquid Water—A New Analysis Tool. *Monthly Weather Review*, 100(7):548–552, 1972. ISSN 00270644. doi: 10.1175/1520-0493(1972)100<0548:VILWNA>2.3.CO;2. URL http://journals.ametsoc.org/doi/abs/10.1175/1520-0493%281972%29100%3C0548%3AVILWNA%3E2.3.CO%3B2.

Pieter Groenemeijer, Zhongjian Liang, Bernold Feuerstein, Susanne Haeseler, Alois M Holzer, and Thilo Kühne. European Severe Storms Laboratory. 2011. URL http://essl.org/ESWD/http://eswd.eu.

Iwan Holleman. Hail Detection using Single-Polarization Radar. *Knmi Wr-2001-01*, page 72, 2001. URL http://www.knmi.nl/publications/fulltexts/wr_hail.pdf.

R Jewell and J C Brimelow. Evaluation of an {Alberta} Hail Growth Model Using Severe Hail Proximity Soundings from the United States. *Wea. Forecasting*, 24(1977):1592–1609, 2009. ISSN 0882-8156. doi: 10.1175/2009WAF2222230.1.

AW Johnson and KE Sugden. Evaluation of Sounding-Derived Thermodynamic and Wind-Related Parameters Associated with Large Hail Events. *E-Journal of Severe Storms Meteorology*, 9(5):1–42, 2014. URL http://www.ejssm.org/ojs/index.php/ejssm/article/viewArticle/137.

J. T. Johnson, Pamela L. MacKeen, Arthur Witt, E. De Wayne Mitchell, Gregory J. Stumpf, Michael D. Eilts, and Kevin W. Thomas. The Storm Cell Identification and Tracking Algorithm: An Enhanced WSR-88D Algorithm. *Weather and Forecasting*, 13(2):263–276, 1998. ISSN 0882-8156. doi: 10.1175/1520-0434(1998)013<0263:TSCIAT>2.0.CO;2.

Thomas Junghänel, Christoph Brendel, Tanja Winterrath, and Andreas Walter. Towards a radar- and observation-based hail climatology for Germany. *Meteorologische Zeitschrift*, 25(4):435–445, 2016. ISSN 16101227. doi: 10.1127/metz/2016/0734.

Vitaly I. Khvorostyanov and Judith a. Curry. Fall Velocities of Hydrometeors in the Atmosphere: Refinements to a Continuous Analytical Power Law. *Journal of the Atmospheric Sciences*, 62(12):4343–4357, 2005. ISSN 0022-4928. doi: 10.1175/JAS3622.1.

Robert C Miller. jljbjiJJjj ANALYSIS AND SEVERE-STORM THE AIR FORCE By. (May), 1972.

J. R. Probert-Jones. The radar equation in meteorology. *Quarterly Journal of the Royal Meteorological Society*, 88(378):485–495, 10 1962. ISSN 00359009. doi: 10.1002/qj.49708837810. URL http://doi.wiley.com/10.1002/qj.49708837810.

Tomáš Púčik, Pieter Groenemeijer, David Rýva, and Miroslav Kolář. Proximity Soundings of Severe and Nonsevere Thunderstorms in Central Europe. *Monthly Weather Review*, 143(12):4805–4821, 2015. ISSN 0027-0644. doi: 10.1175/MWR-D-15-0104.1. URL http://journals.ametsoc.org/doi/abs/10.1175/MWR-D-15-0104.1%5Cnhttp://journals.ametsoc.org/doi/10.1175/MWR-D-15-0104.1.

Roland Stull. *Practical Meteorology: an algebra based survey of atmospheric science*. 2016. ISBN 9780888651761. URL http://doer.col.org/handle/123456789/5710.

G J Stumpf, T M Smith, and J Hocker. New hail diagnostic parameters derived by integrating multiple radars and multiple sensors. *Preprints, 22nd Conf. on Severe Local Storms, Hyannis, MA, Amer. Meteor. Soc. P*, 7(January), 2004.

Mateusz Taszarek, Harold E. Brooks, and Bartosz Czernecki. Sounding-Derived Parameters Associated with Convective Hazards in Europe. *Monthly Weather Review*, 145(4):1511–1528, 2017. ISSN 0027-0644. doi: 10.1175/MWR-D-16-0384.1. URL http://journals.ametsoc.org/doi/10.1175/MWR-D-16-0384.1.

Aarnout Van Delden. The synoptic setting of thunderstorms in Western Europe. *Atmospheric Research*, 56(1-4):89–110, 2000. ISSN 01698095. doi: 10.1016/S0169-8095(00)00092-2.

A. Waldvogel, W. Schmid, and B. Federer. The kinetic energy of hailfalls. Part I: Hailstone spectra, 1978. ISSN 0021-8952.

A Waldvogel, B Federer, and P Grimm. Criteria for the Detection of Hail Cells, 1979. ISSN 0021-8952.

Arthur Witt, Michael D. Eilts, Gregory J. Stumpf, J. T. Johnson, E. De Wayne Mitchell, and Kevin W. Thomas. An Enhanced Hail Detection Algorithm for the WSR-88D. *Weather and Forecasting*, 13(2):286–303, 1998. ISSN 0882-8156. doi: 10.1175/1520-0434(1998)013<0286:AEHDAF>2.0.CO;2.

Sandra Yuter. Precipitation Radar. *Encyclopedia of Atmospheric Sciences*, pages 1833–1851, 2003. doi: 10.1016/B978-0-12-382225-3.00328-5.